Curvature Spectra and Nongaussianities in the Roulette Inflation Model of the Early Universe

Aaron C. Vincent

Master of Science

Department of Physics

McGill University

Montreal,Quebec

2008-08-08

A thesis submitted to McGill University in partial fulfilment of the requirements of the degree of Master of Science

ACKNOWLEDGEMENTS

I would like to thank Niayesh Afshordi, Neil Barnaby, Robert Brandenberger, Francis-Yan Cyr-Racine, Keshav Dasgupta, Paul Franche, Andrew Frey, Anke Knauf, Jean Lachapelle, Nima Lashkari, Larissa Lorenz, Sergei Prokushkin, Gerasimos Rigopoulos, James Sully, Andrew Stewart and Licia Verde for their fruitful input and discussions. Special thanks go to my supervisor Jim Cline, for providing valuable insight and for carefully checking my calculations. This work was partially supported by the Fonds québécois de la recherche sur la nature et les technologies (FQRNT).

ABSTRACT

We explore the "Roulette Inflation" model, a variety of two-field Kähler moduli inflation scenario with a nonstandard kinetic term derived from Type IIB string theory in the large-volume compactification. We provide an overview of the model and the cosmological tools used to compute observables. Our calculations show that entropy perturbations can account for up to 90% of $P_s(k)$ at COBE scales. We further show that the effective single-field result over-estimates the scalar spectral index; a full calculation predicts a slightly red-shifted spectrum $0.92 \lesssim n_s \lesssim 0.98$. Calculation of nongaussianity from the superhorizon evolution of adiabatic modes shows that for most trajectories examined, Roulette inflation predicts small, positive f_{NL}, which would be unmeasurable by the upcoming 9-year WMAP data and the Planck mission. Should they be detectable, momentum-dependent bispectra would provide a good discriminator between models and inflationary trajectories within models.

ABRÉGÉ

Nous étudions le modèle d'inflation de type "Roulette", un modèle basé sur la relaxation de modules de Kähler sur une variété Calabi-Yau, ayant un terme cinétique non-trivial et provenant de la théorie des cordes de Type IIB, dans le contexte de la compactification à grand volume. Nous démontrons que l'influence des perturbations d'entropie peuvent compter pour jusqu'à 90% de $P_s(k)$ à l'échelle de COBE. Nous démontrons que le résultat effectif provenant de la théorie à un seul champ surestime n_s; un calcul complet prédit un spectre décalé vers le rouge $0.92 \lesssim n_s \lesssim 0.98$. Nous calculons finalement la non-gaussianité des perturbations adiabatiques résultant de leur évolution à l'extérieur du rayon de Hubble, et arrivons à des prédictions de $f_{NL} \ll 1$, ce qui ne serait pas mesurable par les observations des prochaines années. Toutefois, s'il s'avère possible de détecter un bispectre dépendant du nombre d'onde k, ceci servirait d'excellent moyen de différentier divers modèles d'inflation.

TABLE OF CONTENTS

LIST OF TABLES

LIST OF FIGURES

CHAPTER 1

Introduction

The theory of cosmic inflation is arguably one of the greatest successes of modern theoretical cosmology. In addition to providing an elegant solution to the shortcomings such as the flatness problem, the horizon problem and structure formation problem which plague standard big bang cosmology, it provides a graceful and precise prediction of the distribution of anisotropies in the 2.7K cosmic microwave background radiation, and consequently to the distribution of clusters of galaxies on the largest scales in the universe.

However, these successes are so far at the phenomenological level. Ultimately one would like to identify the specific inflation theory, derived from a fundamental theory, which gave rise to our universe. The observation of non-standard features, like a nongaussian component in the spectrum of primordial fluctuations, would provide a powerful discriminator between models.

Recent advances in vacuum stabilization in string theory, most notably the KKLT [19] and the large volume [15] varieties, have put stringy realizations of inflation on a much firmer footing. Only when all moduli have been stabilized does it make sense to study which of them might be candidates for inflation. String theory provides an abundance of moduli fields, for example the size and shape of the extra dimensions, and thus many potential opportunities for

inflation. These include single-field models, such as ref. [14], and multiple-field models such as the racetrack [6] or the N-flation scenario [17]. Multiple field inflation has the advantage of more easily providing some of the nonstandard observational features that one would like for helping to discriminate between theories. The extra degrees of freedom allow the production of isocurvature modes (perturbations transverse to classical trajectory) and it has become apparent [35] that these may give rise to large nongaussianities in the cosmic microwave background (CMB) temperature fluctuations.

One such model is the Roulette scenario [7], in which the Calabi-Yau manifold (the compactified extra dimensions of string theory) relaxes from an initial excited state towards a minimum of its potential. The large volume compactification that is used ensures that this minimum exists for large ranges of the microscopic parameters. In addition, unlike KKLT, it does not require tuning the constant term in the superpotential to very small values, and it gives a natural expansion parameter, the inverse volume $1/\mathcal{V}$, providing a controlled α' expansion. The last four-cycle and its axionic partner to relax act as slow rolling scalar fields which drive the final stage of inflation.

We will show, through numerical solution of the field equations, that the potential corresponding to a generic, wide range of compactification parameters gives a large region of initial conditions for which the slow roll conditions are satisfied, and inflation occurs, with the prediction of observable parameter values in accordance with known results from CMB and large scale structure survey data. We specifically aimed to explore the region of allowable inflation within Roulette inflation, bounded by the threshold needed to achieve a minimum amount of inflation, and a maximum set by the region in which the universe exists in a regime of stochastic self-reproduction. Specializing to a specific set of microscopic parameters, we explored the various trajectories of

inflation available within the context of this two-field model, and compared our results to a more generic two-field quadratic inflation model. The influence of isocurvature perturbations, which seed inhomogeneieties between the species of fields driving inflation, was found to be quite important.

In addition, recent claims of detection of nongaussianity in the WMAP CMB data, specifically a nonvanishing nonlinearity parameter f_{NL} [44] have sparked a large interest in deviations from gaussianity in the spectrum of primordial fluctuations as an additional observable that must be predicted by a successful theory of the early universe. Given that precision measurements of f_{NL} from experiments such as Planck will soon be available, it is all the more important that the mechanisms governing the production and evolution of primordial nongaussianities be well understood.

Chapter 2 will provide an overview of the string theory behind the Roulette inflation model before addressing the model itself. We will also discuss some of the shortcomings of the model, from a string-theoretical point of view. Chapter 3 will provide an introduction to the classical theory of inflation, followed by an illustration of the mechanism by which an inflationary universe generates inhomogeneieties. We will further differentiate curvature (adiabatic) and isocurvature (entropy) perturbations of the spacetime metric, and will provide a definition and discussion of the nonlinearity parameter f_{NL}, which is the most widely-used tool in the modern literature in the context of quantifying primordial nongaussianity. Section 3.3 will discuss the gradient expansion formalism we will use to approach the calculation of observables in the context of Roulette inflation. Finally, Chapter 4 will contain the results of the numerical analyses carried out with the method of 3.3.

CHAPTER 2

Roulette (Kähler Moduli) inflation

The Roulette model is a string theoretic inflationary scenario set in the context of a Type IIB large volume compactification. Although there may be evolution of several Kähler moduli, the observable part of inflation is governed by last (and lightest) one to relax. Since the earlier-evolving moduli stabilize to deep minuma, they rapidly decouple from the dynamics [7], before the final 60 e-foldings. The name "roulette" comes from the cyclic shape of the potential, resembling a roulette table whose grooves are the minima toward which the inflaton eventually relaxes (fig. 2–1). During inflation, the F-term potential of the large volume compactification is flat enough to allow slow-rolling over sizeable patches of field space. Reheating, which we will not address here, occurs when the inflaton fields oscillate at the bottom of the potential. This model was first proposed as a single-field inflation model by Conlon and Quevedo in [14], and subsequently generald to include the axion as a second inflaton field by Bond, Kofman, Prokushkin and Vaudrevange in ref. [7].

As in ref. [7], we use the large-volume compactification [15], in which the 10 spacetime dimensions of type IIB string theory are separated into a 4-dimensional noncompact spacetime and a conformally Calabi-Yau 3-fold.

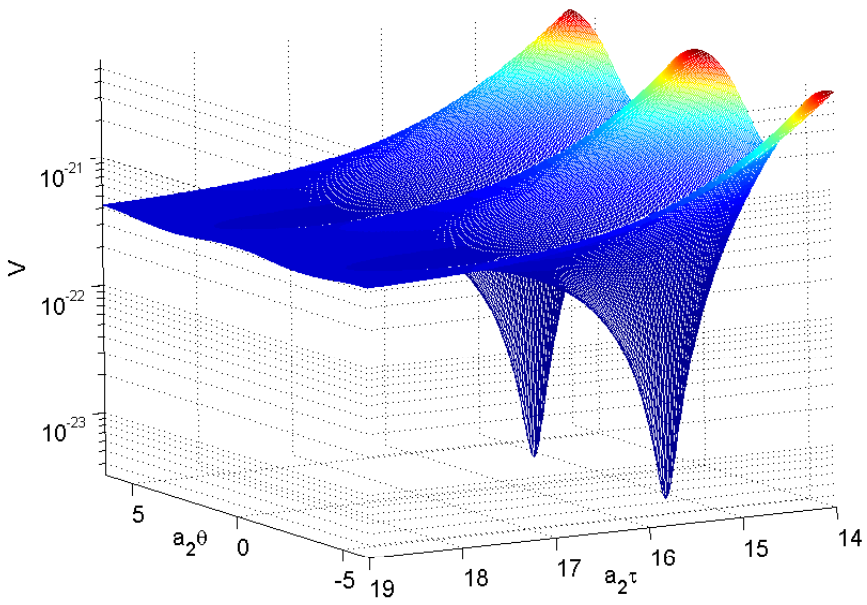

Figure 2–1: The potential (2.21) as of function of the volume modulus τ and its axionic partner θ for parameter set 1.The structure is periodic in the θ direction.

This compactification contains O3/O7 orientifold planes, D3/D7 branes and fluxes which contribute to the stabilization of the compact manifold [15]. Only two Hodge numbers are needed to describe such a manifold: $h^{1,1}$ and $h^{2,1}$. These correspond to the number of Kähler moduli and complex structure (CS) moduli, respectively. While the latter can be seen as specifying the overall shape of the manifold, the former, whose elements we shall call T^i, can be thought of as describing the overall sizes of the cycles which make up the manifold. We will consider the CS moduli, along with the dilaton, to have been dynamically fixed at their global minima, and shall treat the real and imaginary parts of $T_i = \tau_i + i\theta_i$ as independent dynamic fields. τ_i corresponds to the four-cycle volume modulus, while θ_i is its axionic parter, arising from the Ramond-Ramond four-form on the manifold [15]. The only additional

requirement is that $h^{2,1} > h^{1,1} > 1$. The Kähler potential is:

$$K = \frac{\mathcal{K}}{M_P^2} = -2\ln\left(\mathcal{V} + \frac{\xi}{2}\right) + \mathcal{K}_{cs}. \tag{2.1}$$

Here $\mathcal{K}_{cs}$ is an irrelevant constant since it depends on the CS moduli, which are assumed to be heavy. ξ arises from α'^3 corrections and is essential for obtaining the large-volume compactification [15]; it is related to the Euler characteristic of the potential by $\xi = -\frac{\zeta(3)\chi(M)}{2(2\pi)^3}$ and may be expressed in terms of the Hodge numbers through $\chi(M) = 2(h^{1,1} - h^{2,1})$. It should be noted that there has been substantial disagreement [5, 13] about additional correction terms to the Kähler potential within the large volume scenario of the form:

$$\sum_{i=1}^{h^{1,1}+1} \frac{\mathcal{E}_i^{(K)}}{S_1\tau_i} + \sum_{i\neq j\neq k}^{h^{1,1}+1} \frac{\mathcal{E}_i^{(W)}}{\tau_i\tau_j}. \tag{2.2}$$

where the sum runs over the Kähler moduli and the dilaton; $\mathcal{E}_i^{(K)}$ and $\mathcal{E}_i^{(W)}$ are unknown functions of the complex structure and open string moduli and S_1 is the real part of the dilaton. The first sum originates from the exchange of Kaluza-Klein modes between D7-branes and D3 branes (or O7 planes and O3 planes) that are localized within the internal space. The second term, proportional to $1/\tau^2$, originates from the exchange of winding strings between stacks of D7-branes, and their existence depends on the topology of specific cycles within the model under consideration.

Although the terms proportional to the dilaton and to the overall volume $(1/\tau_1)$ should be suppressed and therefore unimportant, it should be stressed that these terms could potentially spoil the overall flatness of the model, rendering slow-roll inflation unsustainable. It has been claimed in ref. [5] that

these corrections are "likely" to be of the form:

$$\sum_{i}^{h^{1,1}+1} \frac{g_K^i \mathcal{E}_i^{(K)}}{S_1 \mathcal{V}} \tag{2.3}$$

and

$$\sum_{i}^{h^{1,1}+1} \frac{g_W^i \mathcal{E}_i^{(W)}}{\mathcal{V}} \tag{2.4}$$

respectively, where g_K and g_W are functions that determine the scaling of the KK and winding mode corrections. Given that these are volume-suppressed and do not depend explicitly on the Kähler moduli, they would not spoil the F-term potential's flatness. However, ref. [11] points out that these corrections may be avoided by removing the D7 brane from the inflating cycle, which has the disadvantage of complicating the reheating process. Given that in a full string theoretical setup the Standard Model would be most easily located on this brane, a nontrivial mechanism would be needed to transfer energy to another location in the compact internal dimensions during reheating. This could occur via a process akin to the ones studied in multiple-throat inflationary models in warped compactifications. See for instance ref. [3]. Since we will not address reheating here, we will assume that these corrections are avoided for the purposes of model-building.

The volume of the Calabi-Yau manifold can be written in terms of two-cycle moduli t^i:

$$\mathcal{V} = \frac{1}{6}\kappa_{ijk} t^i t^j t^k, \tag{2.5}$$

where i, j, k range from 1 to $h^{1,1}$ and κ_{ijk} is the triple intersection form of the manifold $\mathcal{M}$. To each two-cycle modulus t^i corresponds a four-cycle modulus τ_i defined through the transformation:

$$\tau_i = \frac{\partial}{\partial t^i}\mathcal{V} = \frac{1}{2}\kappa_{ijk} t^j t^k. \tag{2.6}$$

τ_i coincides with the real part of the Kähler modulus T_i. The matrix $\kappa_{ij} \equiv \frac{\partial^2}{\partial\tau^i\partial\tau^j}\mathcal{V}$ has signature $(1, h^{1,1}-1)$ [7, 9], so the volume may be written as

$$\mathcal{V} = \alpha\left(\tau_1^{3/2} - \sum_{i=2}^{n}\lambda_i\tau_i^{3/2}\right), \tag{2.7}$$

where α and λ_i are model-dependent, positive parameters. This is sometimes referred to as the "swiss cheese" geometry, with one large modulus τ_1 defining an overall volume, and the other moduli specifying the sizes of holes in the manifold. τ_i have units of l_s^4 (l_s being the string length), whereas the volume $\mathcal{V}$ naturally has units of l_s^6.

The standard $\mathcal{N}=1$ supergravity scalar potential is:

$$V(\phi,\bar{\phi}) = e^{\mathcal{K}/M_P^2}\left(\mathcal{K}^{i\bar{j}}D_iWD_{\bar{j}}\overline{W} - \frac{3}{M_P^2}W\overline{W}\right) + \text{D-terms}, \tag{2.8}$$

where i runs over all moduli. The Kähler metric is $\mathcal{K}^{i\bar{j}} = \left(\frac{\partial^2\mathcal{K}}{\partial T^i\partial\overline{T^j}}\right)^{-1}$, and the Kähler derivative is:

$$D_iW \equiv \partial_iW + (\partial_i\mathcal{K})W \tag{2.9}$$

To fix the CS moduli at their supersymmetric minimum we impose the condition that $D_aW = 0$, where a runs over the CS moluli only. Along with the dilaton, these can then be integrated out making the F-term potential independent of these parameters, while leaving the Kähler moduli undetermined [15]. The complete nonperturbative superpotential is then:

$$W = W_0 + \sum_{i=1}^{h^{1,1}} A_ie^{a_iT_i}. \tag{2.10}$$

A_i and a_i are model-dependent constants and the sum runs over the Kähler moduli only. These nonperturbative terms arise from $SU(N)$ gaugino condensation with $a_i = 2\pi/N$, or from D3-brane instantons with $a_i = 2\pi$. [15].

The Kähler potential and superpotential are enough to fully specify an $\mathcal{N} = 1$ supergravity [15] (the gauge kinetic function is not important for the present application). We can thus rewrite the full action in terms of the fields ϕ^i and $\bar{\phi}^i$ and the F-term potential $V(\phi^i, \bar{\phi}^i)$:

$$S_{\mathcal{N}=1} = \int d^4x\sqrt{-g}\left[\frac{M_P^2}{2}R - \mathcal{K}_{i,\bar{j}}D_\mu\phi^i D^\mu\bar{\phi}^j - V(\phi^i, \bar{\phi}^i)\right]. \tag{2.11}$$

The volume is minimized at an exponentially large value in string units, and we assume that all but one of the complex Kähler moduli have dynamically relaxed and are trapped at their respective minima, possibly having driven some prior epoch of inflation whose effects are far outside the observable patch of our universe. The assumption is therefore that τ_2 and θ_2 are the lightest fields in the theory. Imposition of this hierarchy is necessary to ensure that only these fields drive the last (observable) era of inflation before the universe became radiation-dominated. Other models of moduli inflation (see *e.g.* [6, 2]) have made different assumptions about hierarchies between moduli.

For an overall minimum to exist within the large volume compactification, the manifold must satisfy $h^{1,1} > 2$. As in [7] we will assume here that τ_1 is the positive modulus which governs the overall volume, and τ_2 is the lightest remaining modulus, which will provide the inflaton(s). The elements of the Kähler metric are the following:

$$K_{1\bar{1}} = \frac{3\alpha(4\mathcal{V}-\xi+6\alpha\sum_k \lambda_k\tau_k^{3/2})}{4(\frac{\mathcal{V}}{\alpha}+\sum_k \lambda_k\tau_k^{3/2})^{1/3}(2\mathcal{V}+\xi)^2} \quad (2.12)$$

$$K_{1\bar{i}} = -\frac{9\alpha^2(\frac{\mathcal{V}}{\alpha}+\sum_k \lambda_k\tau_k^{3/2})^{1/3}\sqrt{\tau_i}\lambda_i}{2(2\mathcal{V}+\xi)^2} \quad (2.13)$$

$$K_{i\bar{j}} = \frac{9\alpha^2\lambda_i\lambda_j\sqrt{\tau_i\tau_j}}{2(2\mathcal{V}+\xi)^2} \quad (2.14)$$

$$K_{i\bar{i}} = \frac{3\alpha\lambda_i[2\mathcal{V}+\xi+6\alpha\lambda_i\tau_i^{3/2}]}{4(2\mathcal{V}+\xi)^2\sqrt{\tau_i}} \quad (2.15)$$

Inverting this, we find:

$$K^{1\bar{1}} = \frac{4(2\mathcal{V}+\xi)(\mathcal{V}+\alpha\sum_k \lambda_k\tau_k^{3/2})^{1/3}(2\mathcal{V}+\xi+6\alpha\sum_k \lambda_k\tau_k^{3/2})}{3\alpha^{4/3}(4\mathcal{V}-\xi)} \quad (2.16)$$

$$K^{1\bar{i}} = \frac{8(2\mathcal{V}+xi)^2\tau_i(\mathcal{V}/\alpha+\sum_k \lambda_k\tau_k^{3/2})^{2/3}}{4\mathcal{V}-\xi} \quad (2.17)$$

$$K^{i\bar{j}} = \frac{8(2\mathcal{V}+\xi)\tau_i\tau_j}{4\mathcal{V}-\xi} \quad (2.18)$$

$$K^{i\bar{i}} = \frac{4(2\mathcal{V}+\xi)\sqrt{\tau_i}(4\mathcal{V}-\xi+6\alpha\lambda_i\tau_i^{3/2})}{3\alpha(4\mathcal{V}-\xi)\lambda_i} \quad (2.19)$$

Substituting the Kähler metric, along with the superpotential (2.10) and the Kähler potential (2.1) into (2.8) we may write the F-term scalar potential explicitly:

$$\begin{aligned} V(T_1,\ldots,T_n) = {} & \frac{12W_0^2\xi}{(4\mathcal{V}-\xi)(2\mathcal{V}+\xi)^2} + \sum_{i=2}^{n}\frac{12e^{2a_i\tau_i}\xi A_i^2}{(4\mathcal{V}-\xi)(2\mathcal{V}+\xi)^2} + \frac{16(a_iA_i)^2\sqrt{\tau_i}e^{-2a_i\tau_i}}{3\alpha\lambda_2(2\mathcal{V}+\xi)} \\ & + \frac{32e^{-2a_i\tau_i}a_iA_i^2\tau_i(1+a_i\tau_i)}{(4\mathcal{V}-\xi)(2\mathcal{V}+\xi)} + \frac{8W_0A_ie^{-a_i\tau_i}cos(a_i\theta_i)}{(4\mathcal{V}-\xi)(2\mathcal{V}+\xi)}\left(\frac{3\xi}{(2\mathcal{V}+\xi)}+4a_i\tau_i\right) \\ & + \sum_{\substack{i,j=2\\ i<j}}^{n}\frac{A_iA_jcos(a_i\theta_i-a_j\theta_j)}{(4\mathcal{V}-\xi)(2\mathcal{V}+\xi)^2}e^{-(a_i\tau_i-a_j\tau_j)}\big[32(2\mathcal{V}+\xi)(a_i\tau_i+a_j\tau_j \\ & + 2a_ia_j\tau_i\tau_j) + 24\xi\big] + V_{\text{uplift}} \end{aligned} \quad (2.20)$$

After minimizing with respect to all Kähler moduli but $T_2 = \tau_2 + i\theta_2$, the potential can be expressed as a function of $\tau \equiv \tau_2$ and $\theta \equiv \theta_2$. After expanding in powers of $1/\mathcal{V}$ this potential reduces to

$$V = \frac{8(a_2 A_2)^2 \sqrt{\tau} e^{-2a_2\tau}}{3\alpha\lambda_2 \mathcal{V}} + \frac{4W_0 a_2 A_2 \tau e^{-a_2\tau}\cos(a_2\theta)}{\mathcal{V}^2} + \Delta V + O(1/\mathcal{V}^3), \quad (2.21)$$

where ΔV is the uplifting contribution, of order $1/\mathcal{V}^2$ [14], adjusted so that that $V = 0$ at its minimum. It is crucial for the naturalness of Kähler moduli inflation that ΔV depends only very weakly upon τ_2 in the case of interest, where $\tau_1 \gg \tau_2$. Because of this, ΔV is nearly constant during inflation, and the slow-roll condition on τ_2 is easily satisfied. Fig. 2–1 shows the form of the potential.

For notational purposes we define $\phi^1 = \tau \equiv \tau_2$ and $\phi^2 = \theta \equiv \theta_2$.

$$\mathcal{L}_{\text{kin}} = \frac{1}{2} K_{2\bar{2}} \delta_{AB} \partial_\mu \phi^A \partial^\mu \phi^B, \quad (2.22)$$

with the $(2, \bar{2})$ component of the Kähler metric given by

$$K_{2\bar{2}} = \frac{3\alpha\lambda_2[2\mathcal{V} + \xi + 6\alpha\lambda_2\tau_2^{3/2}]}{4(2\mathcal{V} + \xi)^2\sqrt{\tau_2}}. \quad (2.23)$$

CHAPTER 3

The cosmological model

3.1 Inflation and the production of inhomogeneities

3.1.1 The basic inflationary picture

The inflationary paradigm as it is known since its creation in the 1980's owes its success mainly to the elegant resolution of two issues. First, a calculation of the horizon distance [33],

$$D_H = a_0 H^{-1} \simeq \frac{6000}{\sqrt{\Omega z}} h^{-1}\text{Mpc}, \tag{3.1}$$

where a_0 is the scale factor today and $h \sim 0.7$ is the dimensionless Hubble parameter, reveals that the horizon at last scattering (redshift $z \sim 1000$) was on the order $D_H \sim 100$ Mpc, which subtends an angle of about 1 degree on the CMB sky. This means that surveys such as WMAP should observe a multitude of causally diconnected regions, in stark contradiction with the observed uniformity, up to deviations $\Delta T/T \sim 10^{-5}$ of the 2.726K background radiation. This is known as the "horizon problem". The second issue concerns the flatness of the universe. Current observations [22] place the spatial flatness at $\Omega = 1.01 \pm 0.02$. However, the $\Omega = 1$ universe is unstable, meaning that a fine tuning of 1 part in 10^{60} of the flat universe [33] is required to obtain the bounds observed today.

The inflationary paradigm provides an elegant solution to both of these issues. We take an early time classical action

$$S = \int d^3\mathbf{x}\sqrt{-g}\left(\frac{1}{2}R + \mathcal{L}_m\right). \tag{3.2}$$

R is the Ricci scalar corresponding to the (unperturbed) homogeneous and isotropic Friedmann-Robertson-Walker (FRW) spacetime metric $g_{\mu\nu}$, given by the line element:

$$ds^2 = g_{\mu\nu}dx^\mu\,\mathrm{d}x^\nu = -dt^2 + a^2(t)\delta_{ij}dx^i dx^j. \tag{3.3}$$

In units where $8\pi G = 1$, the energy momentum tensor for a perfect fluid is given by the matter component of the Lagrange density $\mathcal{L}_m$:

$$T^{\mu\nu} = \frac{\partial\mathcal{L}_m}{\partial g_{\mu\nu}} - g^{\mu\nu}\mathcal{L}_m = (p+\rho)U^\mu U^\nu + pg^{\mu\nu}, \tag{3.4}$$

where U^μ is the fluid's four-velocity, ρ is its energy density and p is its pressure. The trace component of the corresponding Einstein equations, which corresponds to the equation of motion for the scale factor $a(t)$ becomes the first Friedmann equation:

$$\ddot{a} = -\frac{1}{6}(\rho + 3p)a, \tag{3.5}$$

while, in the gauge chosen in (3.3), the second Friedmann equation is:

$$H^2 \equiv \left(\frac{\dot{a}}{a}\right)^2 + \frac{k}{a^2} = \frac{\rho}{3}. \tag{3.6}$$

If $\rho + 3p < 0$, this gives rise to a positive acceleration $\ddot{a}$, and therefore to an accelerated uniform expansion of spacetime. If the particular solution $p = -\rho$ is valid for a sufficient amount of time (meaning $H \simeq const.$), we obtain by solving (3.6):

$$a(t) = a_0 e^{Ht}, \tag{3.7}$$

where a_0 is the scale factor at some time $t = t_0$. This corresponds to a *de Sitter* universe. Such an expansion would have the benefit of removing "classical hairs," or inhomogeneities that would have existed prior to inflation by "expanding them away", and would also allow large scales in the sky to have been correlated at early times, solving the horizon problem. The flatness problem is solved in a similar way, via the second Friedmann equation (3.6), which we rescale in terms of $\Omega = \rho/\rho_c$. $\rho(t)$ is the energy density of the universe, while ρ_c is the critical density at which the universe is spatially flat. The curvature today Ω_0 can be written in terms of an initial curvature Ω_i:

$$\Omega_0 = 1 + (\Omega_i - 1)\left(\frac{\dot{a}_i}{\dot{a}_0}\right)^2. \tag{3.8}$$

In the case of the exponentially expanding universe, $\Omega_0 = 1$ is therefore an attractor solution and the flat spatial curvature occurs naturally and without the need for fine tuning for $\Omega_i \sim 1$.

The most common way to obtain $\rho + 3p < 0$ is through the introduction of one or several slowly varying classical scalar fields ϕ^A whose energy we assume to have dominated the universe at early times. If $\mathcal{L}_m = -\frac{1}{2}\partial^\mu\phi\partial_\mu\phi - V(\phi)$, then the corresponding pressure and density are:

$$\rho = \frac{1}{2}\dot{\phi}^2 + V(\phi) + \frac{1}{2}(\nabla\phi)^2, \tag{3.9}$$

$$p = \frac{1}{2}\dot{\phi}^2 - V(\phi) - \frac{1}{6}(\nabla\phi)^2. \tag{3.10}$$

If the kinetic and gradient terms are small enough, this gives the equation of state $\rho = -p$, thus leading to the de Sitter solution. In models of so-called new and chaotic inflation, the kinetic term is taken to be small but non-zero, and the field is taken to roll slowly towards a minimum $V(\phi_{min}) = 0$ in

the potential, ensuring a "graceful exit" from inflation and giving way to a radiation-dominated universe via the decay of the inflaton field.

Within this framework, another important aspect of inflation can be realized: the production of primordial inhomogeneieties with a near scale-invariant power spectrum, which is arguably the greatest success of inflationary theory. Particle production from quantum fluctuations is guaranteed to be observed in a time-dependent background and is important in an accelerated frame with a horizon. Quantum mechanically, this is easiest seen in terms of the conformal time η [32] defined such that $ds^2 = a^2(\eta)(-d\eta^2 + d\mathbf{x}^2)$, for the region $\infty < \eta < 0$. For illustrative purposes we take a simple quadratic model of inflation, where $V(\phi) = \frac{1}{2}m^2\phi^2$ corresponding to a classically rolling free field with mass squared m^2. We take ϕ to start at some finite, non-equilibrium value $\phi_i \neq 0$. Making the further substitution $\chi \equiv a(\eta)\phi$, the action (3.2) becomes [1] :

$$S = \int d^3\mathbf{x}\, d\eta \, \left[\frac{1}{2}\chi'^2 - \frac{1}{2}(\nabla\chi)^2 - \left(m^2a^2 - \frac{a''}{a}\right)\chi^2\right] \tag{3.11}$$

Varying this action with respect to χ gives the equation of motion:

$$\chi'' - \nabla^2\chi + \left(m^2a^2 - \frac{a''}{a}\right)\chi = 0. \tag{3.12}$$

This is identical to the familiar Klein-Gordon equation for a scalar field, but with a time-varying "mass" term. We therefore expect the solution on small scales to similar to a harmonic oscillator. In momentum space, this becomes:

[1] For the remainder of this section, primes will denote differentiation with respect to conformal time η, whereas dots will denote differentiation with respect to coordinate time t.

$$\chi_k'' + \left(k^2 + m^2 a^2(\eta) - \frac{a''(\eta)}{a(\eta)}\right)\chi_k = 0, \tag{3.13}$$

where

$$\chi(\mathbf{x},\eta) = \int \frac{d^3\mathbf{k}}{(2\pi)^{3/2}}\ \chi_k\ e^{i\mathbf{k}\cdot\mathbf{x}}. \tag{3.14}$$

If the acceleration of a is positive, two regimes can readily be identified. When the "mass"

$$m_{\text{eff}} \equiv k^2 + m^2 a^2(\eta) - \frac{a''(\eta)}{a(\eta)} \tag{3.15}$$

is positive, that is on very small length scales, this is akin to the harmonic oscillator in Minkowski space, and we therefore expect the spectrum to behave as such. On larger length scales, however, the a-dependence becomes important. This in turn amounts to time dependence of the mass term, which corresponds to a time-dependence of the system's Hamiltonian in the Heisenberg picture. If the vacuum state is defined as the lowest-energy eigenstate of the Hamiltonian, the latter's time-dependence means that even if the universe is in an initial vacuum state $|0\rangle$, a time Δt later $|0\rangle$ will no longer correspond to a vacuum state. To an observer, this looks like particle creation and is indeed the mechanism that is believed to have seeded the primordial inhomogeneities from inflation.

On large, "superhorzion" scales ($k^{-1} \gtrsim H^{-1}$, where the Hubble length H^{-1} is the natural length scale under consideration), these inhomogeneieties can be treated as classical, stochastically-sourced perturbations on top of the classically rolling inflaton field (see *e.g.* ref.[34]); once they have grown larger than the horizon scale, these fluctuations decohere and become essentially deterministic. This classical evolution will be the subject of the next chapter. The scale of these perturbations at horizon crossing, however, is set by

matching the results of the quantum evolution within the horizon with the superhorizon solution. We will give a rough sketch of this mechanism following the treatment of Ref. [32]. To this effect, we first promote χ and its conjugate momentum $\pi \equiv \chi'$ to operators satisfying the usual commutation relations [32]:

$$[\hat{\chi}(\mathbf{x},\eta), \hat{\pi}(\mathbf{y},\eta)] = i\delta^3(\mathbf{x}-\mathbf{y}); \tag{3.16}$$

$$[\hat{\chi}(\mathbf{x},\eta), \hat{\chi}(\mathbf{y},\eta)] = [\hat{\pi}(\mathbf{x},\eta), \hat{\pi}(\mathbf{y},\eta)] = 0. \tag{3.17}$$

We then expand the field $\hat{\chi}$ in terms of creation and annihilations operators $\hat{a}^{\pm}_{\mathbf{k}}$:

$$\hat{\chi} = \frac{1}{\sqrt{2}} \int \frac{d^3\mathbf{k}}{(2\pi)^{3/2}} \left(e^{i\mathbf{k}\cdot\mathbf{x}} v_k^*(\eta) \hat{a}^-_{\mathbf{k}} + e^{-i\mathbf{k}\cdot\mathbf{x}} v_k(\eta) \hat{a}^+_{\mathbf{k}} \right). \tag{3.18}$$

The mode functions $v_k(\eta)$ then obey the equations of motion:

$$v_k'' + \omega_k^2(\eta) v_k = 0, \tag{3.19}$$

where $\omega_k(\eta) \equiv \sqrt{k^2 + m^2_{\text{eff}}(\eta)}$ and m_{eff} was defined in (3.15). The amplitude of χ is therefore found by solving for the modes v_k, which obey the normalization condition:

$$\frac{v_k' v_k^* - v_k v_k^{*'}}{2i} = 1. \tag{3.20}$$

For a de Sitter universe we write (3.7) in terms of conformal time: $a(\eta) = -1/H\eta$ for $-\infty < \eta < 0$. Then (3.19) becomes [32, 31]:

$$v_k'' + \left[k^2 - \left(2 - \frac{m^2}{H^2} \right) \frac{1}{\eta^2} \right] v_k = 0. \tag{3.21}$$

With a further change of variables [32] $s \equiv k|\eta|$, $v_k \equiv \sqrt{s} f(s)$, eq. (3.21) reduces to the Bessel equation:

$$s^2 \frac{d^2}{ds^2} f(s) + s \frac{d}{ds} f(s) + (s^2 - n^2) f(s) = 0, \tag{3.22}$$

where $n^2 \equiv \frac{9}{4} - \frac{m^2}{H^2}$. This is solved exactly via the Bessel functions:

$$\begin{aligned} f(s) &= AJ_n(s) + BY_n(s) : && (3.23) \\ J_n(s) &\equiv \sum_{m=0}^{\infty} \frac{(-1)^m}{m!\Gamma(m+n+1)} \left(\frac{s}{2}\right)^{2m+n}, && (3.24) \\ Y_n(s) &\equiv \frac{J_n(s)\cos(n\pi - J_{-n})}{\sin(n\pi)}. && (3.25) \end{aligned}$$

Therefore:

$$v_k(\eta) = \sqrt{k|\eta|}(A_k J_n(k|\eta|) + B_k Y_n(k|\eta|), \tag{3.26}$$

with n defined above. The normalization condition (3.20) further imposes the constraint:

$$A_k B_k^* - A_k^* B_k = \frac{i\pi}{k}. \tag{3.27}$$

To fix the initial conditions, we are required to choose a vacuum. Far in the past $\eta \to -\infty$: $k|\eta| \gg 1$, Eq. (3.21) is a standard quantum mechanical harmonic oscillator. The vacuum is the minimal excitation state:

$$v_k(\eta \to -\infty) = \frac{1}{\sqrt{\omega_k}} e^{i\omega_k \eta}. \tag{3.28}$$

Using this asymptotic solution, and matching it to the Bessel solution:

$$v_k(\eta) = \sqrt{\frac{\pi|\eta|}{2}} \left(J_n(k|\eta|) - iY_n(k|\eta|)\right). \tag{3.29}$$

This is often written in terms of the Hankel functions, or Bessel functions of the third kind:

$$\begin{aligned} H_n^{(1)}(s) &\equiv J_n(s) + iY_n(s); && (3.30) \\ H_n^{(2)}(s) &\equiv J_n(s) - iY_n(s). && (3.31) \end{aligned}$$

If $m \ll H$, $n = 3/2$. To connect with observables, we may finally write the amplitude of the perturbations about the vacuum $\delta\phi$ in terms of physical wave modes $k_{ph} = k/a$:

$$\delta\phi(k_{ph}) = \frac{1}{2\pi} a^{-1} k^{3/2} |v_k(\eta)|. \tag{3.32}$$

Around the time of horizon-crossing of a given mode $k_{ph} \sim H$ this reduces to:

$$\delta\phi(k_{\rm ph})_* \simeq \frac{H}{\sqrt{(}8\pi)} \left(\frac{k_{ph}}{H}\right)^{3/2} \tag{3.33}$$

where we have used the fact that $|J_n(k_{ph}H^{-1}) - iY_n(k_{ph}H^{-1})| \sim |H_n^{(2)}(1)| = \sqrt{H_{3/2}^{(2)}(1)H_{3/2}^{(1)}(1)} \sim 1$. This approximation will be entirely adequate, given that modes will be coarse-grained at horizon-crossing using a window function $\mathcal{W}(k)$ before their evolution towards the end of inflation is computed. The only further assumption was $m \ll H$ in order to fix n.

Given the minimal coupling that exists between the scalar field and the metric, fluctuations in the field or fields which dominate the universe will inevitably backreact on the metric. By the time of recombination, overdense (positively curved) and underdense (negatively curved, with respect to the average curvature) regions will give rise to acoustic oscillations of the baryoic fluid as pressure competes with gravitation collapse. The photons emitted during this era will be red- and blue-shifted due to a combination of a doppler shift and a graviational shift (Sachs-Wolfe effect) which manifests itself in turn as red- and blue-shift regions of the CMB sky, and as acoustic peaks when decomposed in terms of multipolar moments. This is the origin of the anisotropies observed within the CMB temperature map, as measured by the COBE and WMAP missions, along with many smaller-scale ground- and balloon-based observations. For recent results, see for instance ref. [22]. The scale of these inhomogeneities is of the order $\Delta T/T \sim 10^{-5}$, with a nearly

gaussian distribution. The extent of this gaussianity will be addressed in the next chapter.

In the context of this single-field inflationary scenario, some first-order observable quantities may be derived to connect the theoretical picture with observational evidence, mainly from the CMB temperature maps. The power spectrum $P(k)$ corresponding to perturbations at length scale[2] k^{-1} is defined as:

$$\frac{2\pi^2}{k^3}P(k)\delta^{(3)}(\mathbf{k}_1 - \mathbf{k}_2) = \langle \zeta_{\mathbf{k}_1}\zeta_{\mathbf{k}_2}\rangle, \tag{3.34}$$

where ζ is the curvature perturbation which will be defined in Eq. (3.42). The power spectrum may be parameterized in the folowing way:

$$P(k) = A_s\left(\frac{k}{k_0}\right)^{n_s-1}. \tag{3.35}$$

At the COBE normalization scale ($k_0 = 7.5a_0H_0$) $A_s = 4\times10^{-10}$ [29]. Current measurements from the 5-year WMAP data using a ΛCDM model put the spectral index at $n_s = 0.960 \pm 0.014$ [22]. The contribution of the adiabatic fluctuations to the scalar power spectrum can be written as in [12]

$$P_s(k) = \frac{1}{50\pi^2}\frac{H_*^4}{\mathcal{L}_{\rm kin}} \equiv \delta^2 \tag{3.36}$$

at the scale $k = (aH)_*$, *i.e.,* the * subscript indicates evaluation at time of Hubble radius crossing of the mode with wave number k. There is a conventional factor of $(2/5)^2$ here, to connect with the quantity δ^2 used by observers [29]. It is important to note that this result corresponds to the amplitude of fluctuations at horizon crossing, and therefore underestimates the power spectrum in the presence of isocurvature modes. This effect is addressed in the

[2] We will henceforth drop the subscript "ph". $k \equiv k_{ph}$.

following section and turns out to be significant in multiple-field inflation, in agreement with ref. [24].

Finally, the spectral index is

$$n_s - 1 = \frac{d \ln P}{d \ln k} = -2\epsilon - \frac{1}{\epsilon}\frac{d\epsilon}{dt} = 2\eta - 6\epsilon \tag{3.37}$$

at leading order in the slow roll parameters $\epsilon \equiv \frac{1}{2}\left(\frac{V'}{V}\right)^2$ and $\eta \equiv \frac{V''}{V}$, where primes denote differentiation with respect to the inflaton field ϕ, and where we have again neglected the effect of isocurvature modes.

3.1.2 Entropy perturbations and the conservation of the curvature perturbation

In the following section we will explicitly distinguish the adiabatic (curvature) and entropy (isocurvature) perturbation modes in cosmological physics, as well as discuss an important "conservation law" for large-scale fluctuations that will be useful in the analysis of Roulette inflation observables.

In order to relate primordial fluctuations during inflation to cosmological observables, it is natural to track the perturbation of the spacetime metric during inflation, instead of the inflaton field itself. Perturbing the metric to linear order, we write the line element:[3]

$$ds^2 = -(1+2A)dt^2 + 2a^2(t)D_iB dx^i dt + a^2(t)\left[(1-2\psi)\gamma_{ij} + 2D_iD_jE\right]dx^i dx^j \tag{3.38}$$

Here we have fixed the background gauge, but the perturbation gauge has yet to be fixed. γ_{ij} is the metric of an unperturbed space of curvature κ. D_i are the

[3] Note that we are using physical (cosmic) time t here rather than conformal time η as we were in the previous section.

usual covariant derivatives with respect to this metric. ψ is the dimensionless curvature perturbation on fixed-time hypersurfaces. This is related to the often-used gauge-invariant Bardeen variables [31]:

$$\Phi_L \equiv A - \frac{d}{dt}\left(aB - a^2\dot{E})\right), \tag{3.39}$$

$$\Psi_L \equiv \psi + H\left(a^2\dot{E} - aB\right). \tag{3.40}$$

The subscript "L" denotes the fact that these quantities are linear in perturbation theory. This fact will be important when discussing higher-order effects in section 3.2. The anisotropic stress vanishes to linear order for a scalar field minimally coupled to gravity [18], giving rise to the following constraint:

$$\frac{d}{dt}\left(aB - a^2\dot{E})\right) + H\left(a^2\dot{E} - aB\right) - A + \psi = 0. \tag{3.41}$$

In the longitudinal (or "zero shear") gauge, where $a^2\dot{E}_l - aB_l = 0$, this reduces to $A_l = \psi_l = \Phi_L = \Psi_L$ in the absence of anisotropic stress. This further obviates the need to track all but one of the scalar perturbation variables of (3.38).

We define the curvature perturbation on uniform-density hypersurfaces:

$$-\zeta \equiv \psi + H\frac{\delta\rho}{\dot{\rho}} \tag{3.42}$$

which reduces to the Bardeen potential on uniform-density hypersurfaces. To linear order, the energy and momentum constraints

$$\delta G_{\mu\nu} = \delta T_{\mu\nu} \tag{3.43}$$

may be written explicitly for a scalar field perturbation of physical wavelength λ with comoving wavenumber $k = 2\pi a/\lambda$ [18]. Without specifying a gauge:

$$3H\left(\dot{\psi} + HA\right) + \frac{k^2}{a^2}\left(\psi + H(a^2\dot{E} - aB)\right) = -\frac{1}{2}\delta\rho \tag{3.44}$$

$$\dot{\psi} + HA = -\frac{1}{2}\delta p, \tag{3.45}$$

where we have defined the perturbed energy-momentum tensor for a scalar field to first order:

$$T^{\mu\nu} \rightarrow (p + \delta p + \rho + \delta\rho)U^\mu U^\nu + (p + \delta p)g^{\mu\nu}. \tag{3.46}$$

Here $g_{\mu\nu}$ stands for the perturbed metric (3.38), and the perturbed 3-velocity of the fluid is $U^i = \nabla^i v$.

The pressure perturbation can be split into an adiabatic and an entropic contribution [43]:

$$\delta p = c_s^2\delta\rho + \dot{p}\Gamma, \tag{3.47}$$

where $c_s^2 \equiv \dot{p}/\dot{\rho}$ is the speed of sound squared; and Γ is the entropy perturbation, defined as the displacement between hypersurfaces of uniform pressure and uniform density:

$$\Gamma \equiv \frac{\delta p}{\dot{p}} - \frac{\delta\rho}{\dot{\rho}} \equiv \frac{\mathcal{S}}{H}, \tag{3.48}$$

where we have defined $\mathcal{S}$ as a dimensionless, gauge-invariant parametrization of the entropy perturbation. The distinction between adiabatic and entropy perturbations is quite important, and worth dwelling on. In a universe populated with multiple cosmological particle species X,Y, ..., with number densities n_X, n_Y, ..., we define *adiabatic* modes as perturbations that affect the overall matter content, and thus the geometry, without changing the relative abundances of species:

$$\delta(n_X/n_Y) = 0. \tag{3.49}$$

These modes are also known as *curvature* perturbations. By analogy with (3.48), we can further define the entropy perturbation between two matter quantities X and Y:

$$\mathcal{S}_{XY} \;=\; H\left(\frac{\delta\rho_X}{\dot{\rho}_X} - \frac{\delta\rho_Y}{\dot{\rho}_Y}\right). \tag{3.50}$$

These are perturbations in which the relative abundance of species changes, but which leave the overall curvature unperturbed, hence the common appelation of *isocurvature* modes. Neglecting interactions between species, we may use the continuity equation $\dot{\rho}_X = -3H(p_X + \rho_X)$ for species with constant respective equations of state $p_X = w_X\rho_X$. Dropping the factor of -3,

$$\mathcal{S}_{XY} = \left(\frac{\delta\rho_X}{(1+w_X)\rho_X} - \frac{\delta\rho_Y}{(1+w_Y)\rho_Y}\right). \tag{3.51}$$

One can form a "basis" of perturbations in which any generic perturbation can be expressed. Taking the late-time universe as an example, one can decompose perturbations into baryon, CDM and neutrino isocurvature modes, respectively [25]:

$$\begin{aligned} S_b &\equiv \delta_b - \frac{3}{4}\delta_\gamma \\ S_c &\equiv \delta_c - \frac{3}{4}\delta_\gamma \\ S_\nu &\equiv \frac{3}{4}\delta_\nu - \frac{3}{4}\delta_\gamma \end{aligned} \tag{3.52}$$

where we have defined entropy shifts with respect to the photon perturbations δ_γ, with $\delta_X \equiv \delta\rho_X/\rho_X$ and have used the equations of state $w_\gamma = w_\nu = 1/3$ and $w_b = w_c = 0$. The adiabatic mode is characterized by $S_b = S_c = S_\nu = 0$.

The picture during the inflationary epoch is more subtle. The case that will ultimately interest us is inflation driven by multiple scalar fields ϕ^A with a potential $V(\phi^A)$, *i.e.* multiple species with the same equation of state

$p_A = -\rho_A$. As will be shown in Section 3.3, it is possible to define a field basis in which the same orthogonalization as in eq. (3.52) can be performed. Defining the trajectory-dependent direction of rolling $\tilde{\phi}^1 \equiv \dot{\phi}^A \phi_A / \sqrt{\dot{\phi}^A \dot{\phi}_A}$, one field carries all of the classical kinetic energy and thus essentially dominates the energy density of the universe. Perturbations $\delta\tilde{\phi}^1$ are therefore associated with adiabatic perturbations, whereas perturbations in field space that are orthogonal to $\tilde{\phi}^1$ are associated with the entropy mode (3.48). This decomposition is illustrated in Figure 3–1 for the case of two fields.

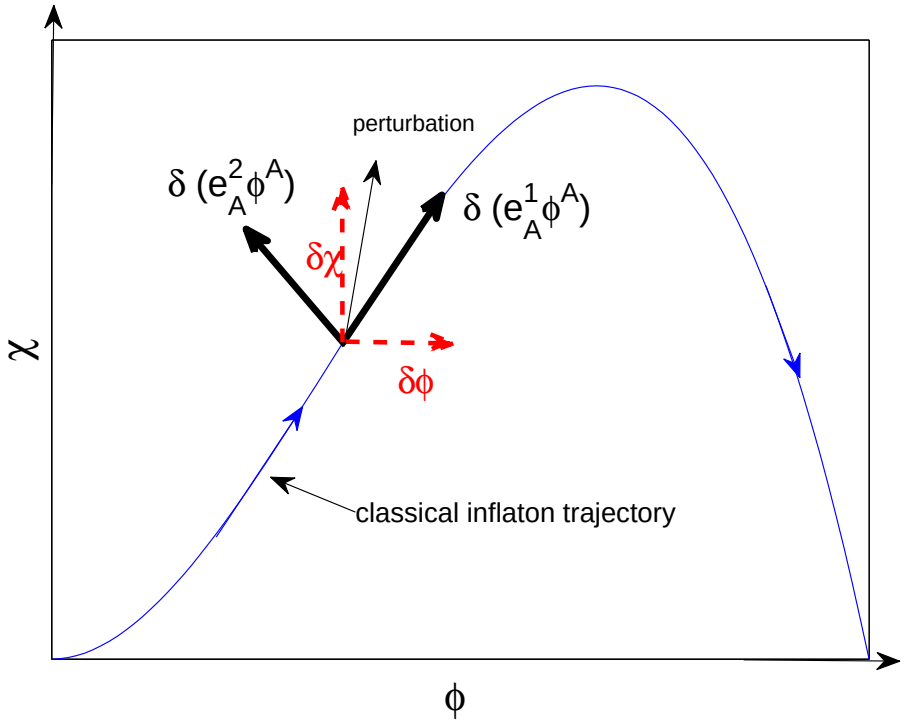

Figure 3–1: The decomposition of perturbations in the context of two-field (ϕ,χ) inflation into a basis of adiabatic (curvature) and entropy (isocurvature) perturbations. The notation used here is that of Section 3.3, where $e^1_A \phi^A \equiv \tilde{\phi}^1$ and $e^2_A \phi^A \equiv \tilde{\phi}^2$.

Independently of these definitions, an important conservation law can be derived which relates the curvature and isocurvature perturbations on large scales, and in fact follows directly from energy conservation $D_\mu T^\mu_\nu = 0$. On

constant physical time hypersurfaces, the curvature perturbation ψ evolves along the unit time-like vector field [43]:

$$n^{\mu} = (1 - A, -\nabla^{i} B). \tag{3.53}$$

Contracting this with the above conservation equation $n^{\mu} D_{\nu} T^{\nu}_{\mu} = 0$, where $T^{\mu\nu}$ to first order in perturbation theory [43]:

$$\dot{\delta\rho} = -3H(\delta\rho + \delta P) + (\rho + p)\left(3\dot{\psi} - \nabla^{2}(\dot{E} + v)\right), \tag{3.54}$$

where we have used the perturbed energy momentum tensor (3.46). In the uniform-density gauge where $\psi = -\zeta$, and $\delta p = \delta p_{\rm nad}$ is the entropy perturbation, (3.54) reduces to:

$$\dot{\zeta} = -\frac{H}{\rho + p}\delta p_{\rm nad} - \frac{1}{3}\nabla^{2}(\dot{E} + v) \tag{3.55}$$

On sufficiently large scales $k^2 \ll (aH)^2$ the gradient term on the right is negligible, and (3.55) becomes a direct proportionality between the evolution of curvature modes on superhorizon scales, and the presence of entropy modes. Although the above long-wavelength conservation law was derived using only first-order perturbation quantities, it was demonstrated in Ref. [28] that it is actually valid exactly if the pressure is a unique function of the energy density. It is often claimed that adiabatic modes are "frozen" once they pass the Hubble scale $(aH)^{-1}$. This statement is only true in models of inflation with generically small entropy perturbations, such as single-field inflationary models. In fact, the remaining term on the right side of (3.55) is very important in the context of multiple-field inflation. As will be argued in Section 3.3, and explicitly illustrated in Chapter 4 for the cases of Roulette and two-field quadratic inflation, this influence can come to dominate the amplitude of the curvature perturbation by the end of inflation.

3.2 Inflation and nongaussianities

Slow-roll inflationary scenarios generically predict a near-scale invariant spectrum of primordial perturbations, with nearly Gaussian statistics. This is expected, since individual quantum fluctuations can be treated as independent results and should therefore be Gaussian by virtue of the central limit theorem. However, more complex field interactions, along with interactions with gravity, which is inherently non-linear, are sure to produce at least small deviations from Gaussianity. Due to the stochastic nature of these perturbations, it is therefore natural to develop statistical tools to compare predictions of the theory with CMB observations. Wick's theorem tells us that the even moments ($2n$-point correlators) of a linear field or distribution ϕ_L decompose into a sum over the permutations of two-point correlators, whereas the odd moments vanish. The measurement of deviations from gaussianity in a field $\phi(\mathbf{x})$, can therefore be made through the bispectrum (the Fourier transform of the three-point correlator), and through the connected part of the trispectrum, that is, the part of the Fourier transform of the four-point correlator that cannot be decomposed into products of the power spectrum.

It is common to parameterize the small deviations from gaussianity in terms of their effect on the Bardeen potential Φ through f_{NL} [23]

$$\Phi(\mathbf{x}) = \Phi_L(\mathbf{x}) + f_{NL}\left(\Phi_L^2(\mathbf{x}) - \langle\Phi_L^2(\mathbf{x})\rangle\right), \tag{3.56}$$

where Φ_L is a purely gaussian random field with $\langle\Phi_L\rangle = 0$. Even for large f_{NL} this parameterisation is sufficient, given that the fluctuations Φ are order $\sim 10^{-5}$. Already with the COBE observations it was shown that the nongaussian fraction of Φ must be less than a few percent, $f_{NL}\langle\Phi_L^2\rangle^{1/2} < 0.04$ (see for example [21]). Subsequent measurements have tightened this limit to the level

Table 3–1: Some recent 95% CL estimates of f_{NL} using WMAP data.

Komatsu *et al.*	(WMAP 1-year)	[21]	$-58 < f_{NL} < 134$
Creminelli *et al.*	(WMAP 3-year)	[16]	$-36 < f_{NL} < 100$
Yadav and Wandelt	(WMAP 3-year)	[44]	$27 < f_{NL} < 147$
Komatsu *et al.*	(WMAP 5-year)	[22]	$-9 < f_{NL} < 111$

of $f_{NL}\langle\Phi_L^2\rangle^{1/2} < 0.003$. Some recent published limits on f_{NL} are shown in table 3–1.

Some of these results [44] suggest that the CMB anisotropies exhibit measurable deviations from Gaussian statistics. Whether or not these detections are confirmed, future observations such as the 9-year WMAP data and the Planck satellite data will provide stringent bounds on the primordial bispectrum, yielding additional parameters that any successful model of the early universe will have to match. Although nongaussianities may be measured from the contribution of any $n > 2$ connected n-point function, the 3-point correlator is the easiest to detect due to the smallness of the anisotropies.

In the original ("local") ansatz (3.56), f_{NL} was taken to be a number, but by relating it to the bispectrum one sees that more generally it could be a function of the momenta k_i. Taking the Fourier transform and writing $\Phi(k) = \Phi_L(k)+\Phi_{NL}(k)$, is easy to show (noting that $\langle\Phi_L^3\rangle$ vanishes identically) that the lowest order nonvanishing component of f_{NL} may be written in terms of the bispectrum and power spectrum:[4]

$$f_{NL} \;\sim\; \delta(\mathbf{k}_1+\mathbf{k}_2+\mathbf{k}_3)\frac{\langle\Phi_L(k_1)\Phi_L(k_2)\Phi_{NL}(k_3)\rangle}{\langle\Phi_L(k_1)\Phi_L(k_2)\rangle^2}. \tag{3.57}$$

[4] One must be careful with the sign of f_{NL}, which has been a source of some confusion in the literature, due to the sign difference between the Bardeen potential and the gravitational potential (see appendix A2 of ref. [27].) We use the WMAP convention that positive f_{NL} corresponds to positive bispectrum of Φ.

A positive value of f_{NL} would lead to a larger number of overdense regions in early universe, which in turn leads to a larger number of cold spots in the CMB map, with respect to the 2.7K background temperature, since overdensities are responsible for redshifting CMB photons through the Sachs-Wolfe effect.[5]

Due to the delta function, the wave vectors form a triangle, and the k-dependence of eq. (3.57) can be expressed in terms of two ratios of momenta, for example k_2/k_1 and k_3/k_1, and an overall scale. Different mechanisms produce bispectra that peak for differently shaped triangles; for example equilateral ($k_1 = k_2 = k_3$), or squeezed ($k_1 \ll k_2 = k_3$). The latter corresponds to the prediction of local ansatz. Single-field slow-roll inflation predicts non-gaussianity of the local type [30], given that the dominant contribution to the bispectrum should come from the superhorizon influence of small k modes which act to "rescale" modes as they evolve toward the end of inflation. A rigorous expansion of the action to third order in perturbation theory is given in ref. [30]. Other models such as ghost inflation and DBI inflation predict large f_{NL} for the equilateral configuration [1], in which non-gaussianities are created before horizon-crossing.

[5] An easy way to visualize the effect of f_{NL} on the sky is through the analogy of the skewness $S_3 \equiv \langle\delta^3\rangle/\langle\delta^2\rangle^2$ of a simple statistical distribution for δ. The median value of a distribution with positive skewness will be slightly larger that its mean $\langle\delta\rangle$, resulting in an asymmetrical distribution. Treating the CMB simply as a coarse-grained set of N pixels, one can in fact get an idea of nongaussianities from the primary skewness S_3 [42, 23]. However, this result is highly dependent on the scale of coarse-graining, and is therefore a much less powerful tool than the full bispectrum.

Although the single-field inflation result is quite important, we will skip the details of this calculation, given that it is quite involved, and we will be interested in a different formalism for the computation of higher-order quantities (see Section 3.3). We merely present the result of Maldacena [30]:

$$\begin{aligned}\langle\Phi(\mathbf{k}_1)\Phi(\mathbf{k}_2)\Phi(\mathbf{k}_3)\rangle &\sim \langle\Phi(\mathbf{k}_1)\Phi(-\mathbf{k}_1)\rangle\frac{1}{\dot{\rho}_*}\frac{d}{dt_*}\langle\Phi(\mathbf{k}_2)\Phi(\mathbf{k}_3)\rangle \qquad (3.58)\\ &\sim (n_{s*}-1)\langle\Phi(\mathbf{k}_1)\Phi(-\mathbf{k}_1)\rangle\langle\Phi(\mathbf{k}_2)\Phi(\mathbf{k}_3)\rangle, \qquad k_1 \ll k_2 \sim k_3.\end{aligned}$$

The subscript $*$ here indicates evaluation at horizon crossing for the rescaled modes k_2 and k_3. Eq. (3.59) is simply a statement that the frozen mode k_1 gives a contribution proportional to the violation in scale-invariance of the two shorter-wavelength modes. It is therefore a prediction of generic single-field inflation that

$$f_{NL} \sim n_s - 1 \ll 1. \qquad (3.59)$$

If the presence of entropy modes during inflation becomes non-negligible, their second-order contribution to the curvature perturbation will give an additional contribution to the superhorizon evolution of curvature modes. Depending on the inflaton trajectory in field space, we will expect this to be the dominant contribution to nonlinear effects in multiple-field inflation. Furthermore, although near-scale invariance guarantees that primordial fluctuations are (nearly) scale-independent, non-linear evolution of the perturbations can result in scale-dependence in the bispectrum. For highly curved trajectories, and hence for large interactions between isocurvature and curvature modes, our results suggest that Roulette inflation indeed exhibits this type of behaviour, albeit quite mildly.

The preceding results indicate that if future experiments confirm claimed detections of $f_{NL} \sim 50$, a large class of single-field inflationary models would be excluded. This has prompted a search for alternate realizations of inflation which would provide not only the required scale-invariant spectrum, but also a large non-gaussian component. Conversely, if future observations are consistent with $f_{NL} = 0$, this will rule out a complimentary set of models, making close proximity to Gaussianity a requirement for model-building.

While some alternatives to inflation, such as the New Ekpyrotic scenario (see, *e.g.* ref.[8]) predict large nongaussianities, most efforts to construct models with large primordial nongaussianities have been from models of inflation. Among these approaches are the inclusion of features in the inflaton potential [10], the use of non-local kinetic terms [4], as well as the use of multiple field inflation to provide a coupling between isocurvature and curvature modes in order to seed a nonvanishing bispectrum. The latter mechanism is the one we will focus on in the context of Roulette inflation.

As a closing remark, we should mention that additional, so-called "secondary" sources of non-linearity can contribute to a measured value of f_{NL} [23]. These foregrounds include Sunyaev-Zel'dovich (SZ) lensing as well as the presence of point sources in the map. These must be carefully computed and subtracted from the $\Delta T/T$ map, as they are caused by late-universe dynamics and structure, rather than inflation itself.

3.3 The gradient expansion formalism

In order to efficiently compute the quantities mentioned above in the context of a multiple-field inflationary model, we will require a complete formalism that can handle both the classical dynamics and the quantum perturbations

that give rise to inhomogeneieties. Our focus will be on tracking the perturbative curvature modes from the time they expand beyond the Hubble radius H^{-1}, until the end of inflation.

The direct expansion of the metric and fields as done above (and as in ref.[18]) makes it easy follow the quantities under consideration, but can turn out to be quite unwieldy when carried out to second order. Another formalism, known as the δN approach [40, 43, 26], has seen widespread use in the computation of second-order quantities (see for example [41, 39]). The premise behind this approach is fairly intuitive: in the uniform density gauge $\delta\rho = 0$, we treat patches of the expanding background spacetime on scales larger than a certain scale $\lambda_0 > H^{-1}$ as separately evolving universes (see Figure 3–2). Curvature perturbations $\Delta\zeta$ are then equal to a difference ΔN in the number of e-foldings for which the universe was locally expanding [43] between two patches a and b:

$$\Delta\zeta \equiv -\psi_a + \psi_b, \tag{3.60}$$

$$\Delta N \equiv N_a - N_b, \tag{3.61}$$

$$\Delta\zeta = \Delta N, \tag{3.62}$$

where N is the duration of inflation in e-foldings. The problem then reduces to computing local perturbations in the duration of inflation.

The approach we will favor here, however, is the gradient expansion approach first introduced in ref. [38] and further developed by Rigopoulos, Shellard and van Tent [36, 35, 37]. The assumptions of homogeneity and isotropy of the background FRW inflationary universe allows the use of the "long-wavelength" approximation, in which the gradient terms of the equations of motion may be dropped in the classical (unperturbed) equations of

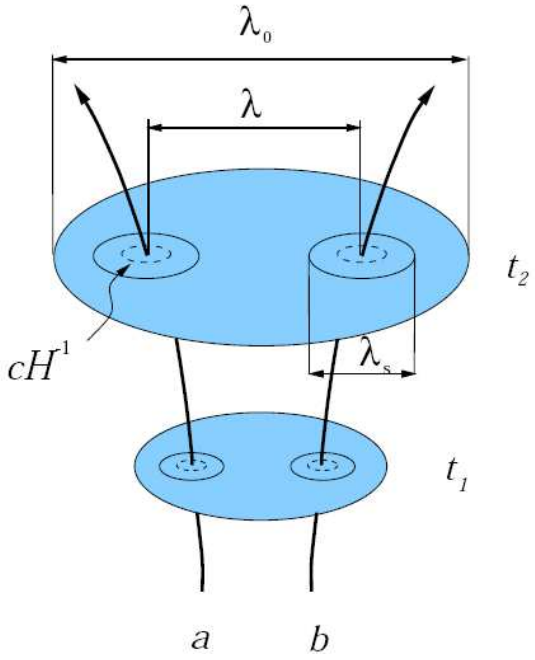

Figure 3–2: The "separate universe" picture used in the context of the δN formalism. Spacelike regions of uniform density $\delta\rho = 0$ and of scale $\lambda > \lambda_s > cH^{-1}$ are taken to evolve independently. λ_0 is the scale below which the homogeneous treatment of the background FRW universe holds. In this picture, the difference in the duration of inflation between regions δN corresponds to the local curvature perturbation. Illustration taken from Wands (2000) [43].

motion (see (3.73), (3.74) and (3.75), below) on scales larger than the Hubble length H^{-1}. This is simply a restatement of the fact that inflation dilutes away classical "hair" that may have been present in the universe before the inflationary epoch.

As a consequence, the inclusion of metric and field perturbations simply amounts to the inclusion of gradient terms on top of the background, whose equations of motion are computed from the full field equations of motion. The advantage of this approach is twofold: no slow-roll approximation is needed to find and solve the equations of motion, and the resulting equations are exact (non-perturbative) results. Quantitative computation of power spectra and

bispectra will require a perturbative expansion of these gradient equations of motion, but this will turn out to be fairly straightforward.

Since the observable quantities that originate from multiple-field inflation are usually highly dependent on the trajectory of the effective inflaton field in field space, we will favor a numerical approach to the solution of the perturbation equations. Analytic results have been developed (e.g. in ref. [35]) in the context of this formalism, but only within certain constrained limits.

Regardless of the specific inflationary model, we may write the action for a general multifield potential $V(\phi_A)$ $(A = 1, 2, ...)$ with minimal gravitational couplings as

$$S = \int d^4x\sqrt{-g}\left(\frac{M_P^2}{2}R - \frac{1}{2}G_{AB}\partial_\mu\phi^A\partial^\mu\phi^B - V(\phi^A)\right). \tag{3.63}$$

Here R is the Ricci scalar, G_{AB} is the metric in field space and $M_P = 1/\sqrt{8\pi G}$ is the reduced Planck mass. We will henceforth work in units where $M_P = 1$. At the homogeneous level, and before specifying a choice of spacelike slicing, the FRW metric is $ds^2 = -N^2(t)\,dt^2 + a^2(t)d\vec{x}^{\,2}$, and varying with respect to the fields ϕ_A, $a(t)$ and $N(t)$ gives the equations of motion for the scalar fields and the Friedmann equations. Here $N(t)$ is the time-lapse function, and $a(t)$ is the scale factor, from which we define the Hubble parameter $H(t) \equiv \dot{a}/(Na)$. To simplify calculations during inflation, we make the coordinate choice

$$t \equiv \ln(a), \tag{3.64}$$

so $N(t) = H^{-1} \simeq$ constant during inflation. Dotted fields will from now on represent differentiation with respect to this time parameter.

Working within the long-wavelength approximation [36], we assume that the fields are homogeneous and isotropic within the horizon, and thus drop

the gradient term from the Lagrange density. The kinetic term becomes:

$$\mathcal{L}_{\rm kin} = \frac{1}{2} G_{AB} \Pi^A \Pi^B, \tag{3.65}$$

having defined the velocities

$$\Pi^A = \frac{\dot{\phi}^A}{N} = H \dot{\phi}^A \tag{3.66}$$

We will furthermore define covariant differentiation of a field that transforms as a vector within field space [36]:

$$D_B L^A = \partial_B L^A + \Gamma^A_{BC} L^C \tag{3.67}$$

$$D_B L_A = \partial_B L_A - \Gamma^C_{AB} L_C \tag{3.68}$$

$$D_\mu L^A = \partial_\mu L^A + \Gamma^A_{BC} \partial_\mu \phi^B L^C \tag{3.69}$$

where Γ^A_{BC} is the connection defined through the metric G_{AB}. Henceforth, uppercase latin indices $A, B, C, ...$ will represent the various fields, greek will represent spacetime indices, and i, j, k will be spatial indices. Since we are interested in a two-field inflation model, $A, B, C, ... = 1, 2$. In the Roulette model there is only one independent connection coefficient:

$$\Gamma^\tau_{\tau\tau} = \Gamma^\theta_{\tau\theta} = \Gamma^\tau_{\theta\tau} = -\Gamma^\tau_{\theta\theta} = \frac{6\alpha\lambda\tau^{3/2} - \mathcal{V}}{4\tau(\mathcal{V} + 3\alpha\lambda\tau^{3/2})} \tag{3.70}$$

$$\Gamma^\theta_{\theta\theta} = \Gamma^\theta_{\tau\tau} = 0 \tag{3.71}$$

For the analysis of the power spectrum and bispectrum, it will furthermore be useful to define the orthonormal basis e^A_m, where $m = 1, 2$:

$$e^A_1 = \frac{\Pi^A}{\Pi}, \qquad e^A_2 = \epsilon_{AB} e^B_1 \tag{3.72}$$

where $\Pi \equiv \sqrt{\Pi_A \Pi^A}$ and ϵ_{AB} is the antisymmetric tensor. e^A_1 is tangent to the classical field trajectory, whereas e^A_2 is orthogonal. Note that lower and

raised indices m, n are equivalent. In the notation we used in Section 3.1.2 $\tilde{\phi}^1 \equiv e^1_A \Pi^A$.

The scalar field equations of motion are [36, 38]:

$$D_t \Pi^A + 3NH\Pi^A = -NG^{AB}V_{,B}, \tag{3.73}$$

$$\partial_t H = -\frac{1}{2} N \, \Pi_A \Pi^A, \tag{3.74}$$

where the Hubble rate (using $M_p = 1$ units) is

$$H^2 = \frac{1}{3}\left(\mathcal{L}_{\rm kin} + V\right), \tag{3.75}$$

We will numerically integrate these equations to determine the inflationary trajectories. The formalism of [35, 36] which we follow makes extensive use of the "slow roll" parameters,

$$\begin{aligned}
\epsilon &= \frac{\Pi^2}{2H^2} = \frac{\mathcal{L}_{\rm kin}}{H^2} \\
\eta^A &= -\frac{3H\Pi^A + G^{AB}\partial_B V}{H\Pi} \\
\eta^{\parallel} &= -3 - \frac{\Pi^A \partial_A V}{H\Pi^2} \\
\eta^{\perp} &= -\frac{e_2^A V_{,A}}{H\Pi} \\
\chi &= \frac{V_{22}}{3H^2} + \epsilon + \eta^{\parallel} \\
\xi_m &= -\frac{V_{m1}}{H^2} + 3(\epsilon - \eta^{\parallel})\delta_{m1} - 3\eta^{\perp}\delta_{m2} \\
\xi^{\parallel} &= \xi_1, \quad \xi^{\perp} = \xi_2
\end{aligned} \tag{3.76}$$

where V_{22} and V_{m1} are defined in the orthonormal basis (3.72), such that $V_{mn} = e^A_m e^B_n V_{;AB}$, with the covariant derivatives over the field metric defined above. These quantities are nonlinear, depend on both t and $\vec{x}$, and are not assumed to be small, although they are small in the slow-roll regime. It should be noted that some of them are unintuitively named; for example $\eta^{\perp}$

is proportional to the slope of the potential, in the direction orthogonal to the trajectory, rather than a curvature, and the relation of $\eta^{\parallel}$ to the usual slow-roll parameters, with respect to the adiabatic direction, is $\eta^{\parallel} = -\eta + \epsilon$. Nevertheless we will keep this notation for ease of comparison with ref. [35]. The ϵ parameter does agree with the conventional ϵ (defined with respect to the slope along the adiabatic direction).

3.4 Computation of the full power spectrum and nongaussianity

We expect the leading contribution to the bispectrum to come from the influence of isocurvature perturbations on the superhorizon evolution of adiabatic modes. We will work in terms of gradient variables of the type:

$$C_i \equiv \partial_i A - \frac{\partial_t A}{\partial_t B}\partial_i B, \tag{3.77}$$

which have the property of being invariant under long-wavelength changes of time-slicing $(t, x) \to (\tilde{t}, \tilde{x})$ [36]. These are the variables that will serve to track the inhomogeneities on top of the homogeneous and isotropic background.

The particular choice of variables we will use to describe the fluctuations in this formalism are

$$\zeta_i^A(t, \mathbf{x}) = e_1^A(t, \mathbf{x})\partial_i \ln a(t, \mathbf{x}) - \frac{1}{\sqrt{2\epsilon(t, \mathbf{x})}}\partial_i \phi^A(t, \mathbf{x}) \tag{3.78}$$

This quantity can be projected onto the field basis (3.72):

$$\zeta_i^m(t, \mathbf{x}) = \delta_{m1}\, \partial_i \ln a - \frac{1}{\sqrt{2\epsilon}} e_{mA}\, \partial_i \phi^A. \tag{3.79}$$

These simplify in the gauge $t = \ln a$, where $\partial_i \ln a = 0$. At first order, ζ_i^1 is the spatial gradient of the usual curvature perturbation, whereas ζ_i^2 corresponds

to the isocurvature perturbation. First, in the gauge $NH = 1$:

$$\begin{aligned} D_t \partial_i \phi^A &= \partial_t \partial_i \phi - \Gamma^A_{BC} \partial_i \phi^B \partial_t \phi^C \\ &= \frac{1}{H} D_i \Pi^A \end{aligned} \tag{3.80}$$

Taking the covariant time derivative of ζ_i^A, and using the equations of motion for the field,

$$\begin{aligned} D_t \zeta_i^A &= \left(\partial_t - \Gamma^A_{BC} \partial_t \phi^B\right) \left(\frac{1}{\sqrt{2\epsilon}} \partial_i \phi^A\right) \\ &= -\frac{2}{(2\epsilon)^{3/2}} (2\epsilon\eta^{\parallel} - 2\epsilon^2) \partial_i \phi^A - \frac{1}{H\sqrt{2\epsilon}} D_i \Pi^A \\ &= 2(\eta^{\parallel} - \epsilon) \zeta_i^A - \frac{1}{H\sqrt{2\epsilon}} D_i \Pi^A \end{aligned} \tag{3.81}$$

Taking the second time derivative is somewhat more involved [36]. This gives, still in the gauge $NH = 1$, the equation of motion for the ζ_i^A:

$$D_t^2 \zeta_i^A - \left(\frac{H}{\dot{H}} - 3 - 2\epsilon - 2\eta^{\parallel}\right) D_t \zeta_i^A + \Xi^A{}_B \zeta_i^B = 0, \tag{3.82}$$

where:

$$\Xi^A{}_B \equiv \frac{V^A_B}{H^2} - 2\epsilon R^A{}_{DCB} e_1^D e_1^C + (3\epsilon + 3\eta^{\parallel} + 2\epsilon^2 + 4\epsilon\eta^{\parallel} + (\eta^{\perp})^2 + \xi^{\parallel}) \delta^A_B - 2\epsilon \left((3 + \epsilon + 2\eta^{\parallel}) e_1^A e_{1B}\right). \tag{3.83}$$

These equations of motion can then be projected onto the field basis, noting that $D_t e^A_m \equiv 0$. The gradients are combined, along with their respective velocities $\theta_i^m \equiv \partial_t \zeta_i^m$, into a 3-component vector,

$$v_{ia} = (\zeta_i^1, \zeta_i^2, \theta_i^2)^T, \tag{3.84}$$

The would-be fourth component is not independent, but is determined to be

$$\theta_i^1 = 2\eta^{\perp} \zeta_i^2 \tag{3.85}$$

by the constraint equations [37] which may be derived from the Einstein equations and the definition of ζ_i^m, noting that $D_t(\partial_i\phi^A) = D_i(N\Pi^A)$:

$$\begin{aligned} \partial_i \ln H &= \epsilon\zeta_i^1, \\ e_{mA}\partial_i\phi^A &= -\sqrt{2\epsilon}\zeta_i^m, \\ e_m^A D_i\Pi_A &= -H\sqrt{2\epsilon}\left(\theta_i^m + \eta^{\parallel}\zeta_i^m - \eta^{\perp}\zeta_i^2\delta_{m1} + (\eta^{\perp}\zeta_i^1 + \epsilon\zeta_i^2)\delta_{m2}\right). \end{aligned} \tag{3.86}$$

The relationship between θ_i^1 and ζ_i^2 is nothing more than the conservation law of the curvature perturbation mentioned in section 3.1.2, This is valid to all orders, as shown in ref. [28].

Combining these with the equations of motion (3.75)-(3.74), the full nonlinear evolution equations may be written in the compact form:

$$\dot{v}_{ia}(t,\mathbf{x}) + A_{ab}(t,\mathbf{x})v_{ib}(t,\mathbf{x}) = 0. \tag{3.87}$$

The matrix A is a function of the parameters defined in eq. (3.76) [37]:

$$A = \begin{pmatrix} 0 & -2\eta^{\perp} & 0 \\ 0 & 0 & -1 \\ 0 & 3\chi + 2\epsilon^2 + 4\epsilon\eta^{\parallel} + 4(\eta^{\perp})^2 + \xi^{\parallel} - 2\epsilon R_{2112} & 3 + \epsilon + 2\eta^{\parallel} \end{pmatrix} \tag{3.88}$$

Its dominant components are $A_{33} \cong 3$ and $A_{23} = -1$. The only explicit dependence on the curvature of the field manifold in A is the term $-2\epsilon R_{2112} \equiv -2\epsilon e_2^A e_1^B e_1^C e_2^D R_{ABCD}$, but we find that this is negligible ($\sim 10^{-6}$) in Roulette inflation.

The next step is to solve this system of equations perturbatively. Eq. (3.87) can be expanded into a hierarchy of linear perturbation equations for $v_{ia}^{(n)}$, each sourced by the previous order. Since we are interested in super-horizon evolution, it is reasonable to take the first-order perturbations to be sourced by a linear perturbation $b_{ia}^{(1)}$, which encodes the effect of quantum

fluctuations at short wavelengths providing the initial values for the long-wavelength modes of interest at horizon crossing. Refs. [35, 36, 37] show that the source term having the right properties is

$$b_{ia}^{(1)} = \int \frac{\mathrm{d}^3\mathbf{k}}{(2\pi)^{2/3}}\, \dot{\mathcal{W}}(k) X_{am}^{(1)} \hat{a}_m^\dagger(\mathbf{k}) i k_i e^{i\mathbf{k}\cdot\mathbf{x}} + \text{c.c.}, \tag{3.89}$$

where the creation operator has the standard commutator $[\hat{a}_m(\mathbf{k}), \hat{a}_n^\dagger(\mathbf{k}')] = \delta_{mn}\delta^{(3)}(\mathbf{k}-\mathbf{k}')$. Superscripts in parentheses indicate the expansion order in perturbation theory.

The matrix of linear solutions around horizon crossing X_{am} is the slow-roll solution of ref. [37] in which it is argued that deviations from linearity on sub-horizon scales should be slow-roll suppressed:

$$X_{am} = -\frac{H}{4k^{3/2}\sqrt{\epsilon}} \begin{pmatrix} 1 & 0 \\ 0 & 1 \\ 0 & -\chi \end{pmatrix}. \tag{3.90}$$

The factor $1/\sqrt{2\epsilon}$ comes from the definition of ζ, and the amplitude H is the result we expect from perturbations at horizon crossing.

The window function $\mathcal{W}(t,k)$ is designed to source only the superhorizon modes, and the final results must be independent of its exact shape. It is convenient to use a Heaviside step function, $\mathcal{W}(t,k) = \Theta(kR-1)$, that has support only on scales $R = (c/aH) = (c/H)e^{-t}$ (recall we are in the gauge $t = \ln a$) sufficiently larger than the Hubble radius, where c should be of order a few. Given that fluctuations that are generated on sub-horizon scales do not yet feel the effect of curvature, and therefore correspond to fluctuations in Minkowski space, it is reasonable to expect the spectrum of fluctuations on these scales to be Gaussian.

Then

$$\dot{\mathcal{W}}(t,k) = \delta(kR-1) = \frac{\delta(t-t_*-\ln c)}{|-ce^{-t+t_*}|}, \tag{3.91}$$

where t_* is the time of horizon-crossing of mode k

$$t_* \equiv \ln k/H_*. \tag{3.92}$$

Physical quantities are found to be independent of the exact value of $c > 1$.

The first- and second-order equations can then be written:

$$\dot{v}^{(1)}_{ia}(t,\mathbf{x}) + A^{(0)}_{ab}(t,\mathbf{x})v^{(1)}_{ib}(t,\mathbf{x}) = b^{(1)}_{ia}, \tag{3.93}$$

$$\dot{v}^{(2)}_{ia}(t,\mathbf{x}) + A^{(0)}_{ab}(t,\mathbf{x})v^{(2)}_{ib}(t,\mathbf{x}) = -A^{(1)}_{ab}(t,\mathbf{x})v^{(1)}_{ib}(t,\mathbf{x}). \tag{3.94}$$

Here, $A^{(1)}_{ab} = \bar{A}^{(0)}_{abc}(t)\partial^{-2}\partial^i v^{(1)}_{ic}$ (note that ∂^{-2} is just multiplication by $-k^{-2}$ in momentum space.) $\bar{A}$ is given by [37]:

$$\bar{A} = \begin{pmatrix} \mathbf{0} & \begin{pmatrix} 2\epsilon\eta^\perp - 4\eta^\parallel\eta^\perp + 2\xi^\perp \\ -6\chi - 2\epsilon\eta^\parallel - 2(\eta^\parallel)^2 - 2(\eta^\perp)^2 \\ -6 - 2\eta^\parallel \end{pmatrix} & \mathbf{0} \\ \mathbf{0} & \mathbf{0} & \mathbf{0} \\ \mathbf{0} & \bar{\mathbf{A}}_{\mathbf{32}} & \begin{pmatrix} -2\epsilon^2 - 4\epsilon\eta^\parallel + 2(\eta^\parallel)^2 - 2(\eta^\perp)^2 - 2\xi^\parallel \\ -4\epsilon\eta^\perp - 2\xi^\perp \\ -2\eta^\perp \end{pmatrix} \end{pmatrix}, \tag{3.95}$$

where

$$\bar{\mathbf{A}}_{\mathbf{32}} \equiv -2\partial_i\epsilon R_{2112} + \begin{pmatrix} \bar{\mathbf{A}}_{\mathbf{321}} \\ \bar{\mathbf{A}}_{\mathbf{322}} \\ \bar{\mathbf{A}}_{\mathbf{323}} \end{pmatrix} \tag{3.96}$$

and

$$\begin{aligned}
\bar{\mathbf{A}}_{\mathbf{321}} &\equiv -6\epsilon\eta^{\parallel} - 6(\eta^{\perp})^2 - 3\epsilon\chi \qquad (3.97)\\
&\quad -4\epsilon^3 - 10\epsilon^2\eta^{\parallel} - 2\epsilon(\eta^{\parallel})^2\\
&\quad -6\epsilon(\eta^{\perp})^2 + 8\eta^{\parallel}(\eta^{\perp})^2 - 3\epsilon\xi^{\parallel}\\
&\quad -6\eta^{\perp}\xi^{\perp} + \sqrt{\frac{\epsilon}{2}}(V_{111} - V_{221})\\
\bar{\mathbf{A}}_{\mathbf{322}} &\equiv -12\epsilon\eta^{\perp} - 6\eta^{\parallel}\eta^{\perp} \qquad (3.98)\\
&\quad +12\eta^{\perp}\chi - 6\epsilon^2\eta^{\perp} + 4(\eta^{\perp})^3\\
&\quad -4\epsilon\xi^{\perp} - 2\eta^{\parallel}\xi^{\perp} + \sqrt{\frac{\epsilon}{2}}(V_{211} - V_{222})\\
\bar{\mathbf{A}}_{\mathbf{323}} &\equiv 6\eta^{\perp} - 2\epsilon\eta^{\perp} + 4\eta^{\parallel}\eta^{\perp} - 2\xi^{\perp} \qquad (3.99)
\end{aligned}$$

The first index in $\bar{A}_{abc}$ stands for the row, the second for the column in (3.95), and the third for the "depth" dimension of the array, represented here by a column vector for each $\bar{A}_{ab}$. V_{lmn} is defined as $V_{lmn} \equiv e_l^A e_m^B e_n^C V_{;ABC}$.

The above linear equations can then be solved with the aid of the Green's function which is the solution to the inhomogeneous equation

$$\frac{\mathrm{d}}{\mathrm{d}t}G_{ab}(t,t') + A^{(0)}_{ac}(t)G_{cb}(t,t') = \delta(t-t'). \qquad (3.100)$$

with $G_{ab}(t,t) = \delta_{ab}$ at equal times. This must be solved only once for each classical trajectory, which we do numerically on a grid in t, t', a and b. Once $G_{ab}(t,t')$ is known, the step-function form of $\mathcal{W}(t,k)$ simplifies the integration of the first order solution,

$$\begin{aligned}
v^{(1)}_{am}(k,t) &= \int_{-\infty}^{t} \mathrm{d}t'\, G_{ab}(t,t')\, \dot{\mathcal{W}}(k,t')\, X^{(1)}_{bm}(k,t')\\
&= G_{ab}(t, t_* + \ln c)\, X^{(1)}_{bm}(k, t_* + \ln c), \qquad (3.101)
\end{aligned}$$

where we have defined the momentum-space perturbation as:

$$v_{ia}^{(1)}(\mathbf{x},t) \;=\; \partial_i v_a^{(1)} = \int \frac{\mathrm{d}^3\mathbf{k}}{(2\pi)^{2/3}}\, v_{am}^{(1)}(k,t)\, a_m^\dagger(\mathbf{k})\, ik_i\, e^{i\mathbf{k}\cdot\mathbf{x}} + \text{c.c.} \quad (3.102)$$

The second order solution can be expressed, using the same method, as:

$$v_{ia}^{(2)}(\mathbf{x},t) = -\int \mathrm{d}t'\, G_{ab}(t,t')\, \bar{A}_{bcd}(t')\, v_{ic}^{(1)}(\mathbf{x},t')\, \partial^{-2}\partial^j v_{jd}^{(1)}(\mathbf{x},t'). \quad (3.103)$$

To connect with observables one transforms the time coordinate t in the gauge of uniform expansion time slices ($NH = 1$) to $T(t,x)$ which describes uniform density slices ($\partial_i\rho = 0$) [37], so $a(t) \to \tilde{a}(T,x)$. Then the curvature perturbation can be expressed as the total gradient of a scalar $\tilde{\alpha}$, $\tilde{\zeta}_i^1 = \partial_i \ln\tilde{a} \equiv \partial_i\tilde{\alpha}$, which allows observable scalar correlators to be expressed simply. Note that this result should be identical to results found using the δN formalism described above, given that the perturbation $\delta\tilde{\alpha}$ in the uniform density gauge corresponds exactly to the perturbation in the number of e-folds $\delta N \equiv \delta \ln\tilde{a} = \zeta$ [43].

The curvature power spectrum is:

$$\mathcal{P}(k,t) = \frac{k^3}{2\pi^2}\langle\tilde{\alpha}\tilde{\alpha}\rangle(k,t) = \frac{k^3}{2\pi^2} v_{1m}^{(1)}(k,t) v_{1m}^{(1)}(k,t). \quad (3.104)$$

The scale-dependence of P comes as expected from the time-dependence of H in $X_{am}(k,t)$ (eq. (3.90)), which appears in $v_{1m}^{(1)}(k,t)$ through eq. (3.101). It should be stressed that the power spectrum here is complete, and because of the influence of isocurvature modes via (3.85) can turn out to be much larger than predicted by (3.36), depending on the inflationary trajectory.

The leading contribution to the bispectrum comes from the expansion to second order in perturbation theory,

$$\begin{aligned}\langle\tilde{\alpha}_{k_1}\tilde{\alpha}_{k_2}\tilde{\alpha}_{k_3}\rangle^{(2)}(t) &= \langle\tilde{\alpha}^{(1)}_{k_1}\tilde{\alpha}^{(1)}_{k_2}\tilde{\alpha}^{(2)}_{k_3}\rangle(t) + (k_1 \leftrightarrow k_3) + (k_2 \leftrightarrow k_3) \qquad (3.105)\\ &= (2\pi)^3\delta^3(\mathbf{k_1}+\mathbf{k_2}+\mathbf{k_3})\,[f(k_1,k_2)+f(k_2,k_3)+f(k_1,k_3)]\end{aligned}$$

where

$$f(k,k') \equiv \left(\frac{1}{2}v^{(2)}_{1mn}(k,k',t) + \eta^{\perp}v^{(1)}_{2m}(k,t)v^{(1)}_{1n}(k',t)\right) v^{(1)}_{1m}(k,t)v^{(1)}_{1n}(k',t) + k \leftrightarrow k'. \qquad (3.106)$$

The second term in parentheses comes from the coordinate change $t \to T$, and the first term is given by

$$v^{(2)}_{1mn}(k,k',t) \equiv -\int_{-\infty}^{t} \mathrm{d}t'\, G_{1a}(t,t')\,\bar{A}_{abc}(t')\,v^{(1)}_{bm}(k,t')\,v^{(1)}_{cn}(k,t'). \qquad (3.107)$$

Numerically, we will find that this term dominates over the $\eta^{\perp}v^{(1)}_{2m}(k,t)v^{(1)}_{1n}(k',t)$ term in the Roulette inflation model by five orders of magnitude. These are all the ingredients needed for evaluation of the nonlinearity parameter f_{NL} [35],

$$f_{NL} = \frac{\langle\alpha^{(1)}_{k_1}\alpha^{(1)}_{k_2}\alpha^{(2)}_{k_3}\rangle + (k_1 \leftrightarrow k_3) + (k_2 \leftrightarrow k_3)}{\langle\alpha^{(1)}\alpha^{(1)}\rangle_{k_1}\langle\alpha^{(1)}\alpha^{(1)}\rangle_{k_1} + (k_1 \leftrightarrow k_3) + (k_2 \leftrightarrow k_3)} \qquad (3.108)$$

CHAPTER 4

Simulation and results

We performed numerical simulations of trajectories that gave inflation within the Roulette model, as well as with the two-field quadratic model, which was first studied in ref. [20]:

$$\mathcal{L} = -\frac{1}{2}(\partial_\mu \phi)^2 - \frac{1}{2}(\partial_\mu \chi)^2 - \frac{1}{2}m_\phi^2 \phi^2 - \frac{1}{2}m_\chi^2 \chi^2, \tag{4.1}$$

where, for comparison with ref. [37] we took $m_\phi = 10^{-5}$ in reduced Planck units, $m_\chi/m_\phi = 12$, with initial conditions $\phi_i = \chi_i = 13$. This gives rise to two successive eras of inflation, with a total of 86 e-folds from start until $\log \epsilon = 0$, separated by a sharp turn in field space, in which the slow roll parameters briefly spike. This trajectory is illustrated in Figure 4–1.

In both of these models, we computed the power spectra, first with (3.36), then with the full numerical result (3.104) which includes the effect of isocurvature modes. The second order solutions $v^{(2)}_{amn}$ were then integrated numerically, allowing the calculation of the bispectrum, and subsequently the non-linearity parameter f_{NL}. This was done for both the equilateral and squeezed forms. The Matlab code for the equilateral computation is included in Appendix A. In the equilateral case, we computed the evolution of f_{NL} for a large range of modes (corresponding to a time of horizon exit $t_*(k)$ from 15 to 70 e-folds

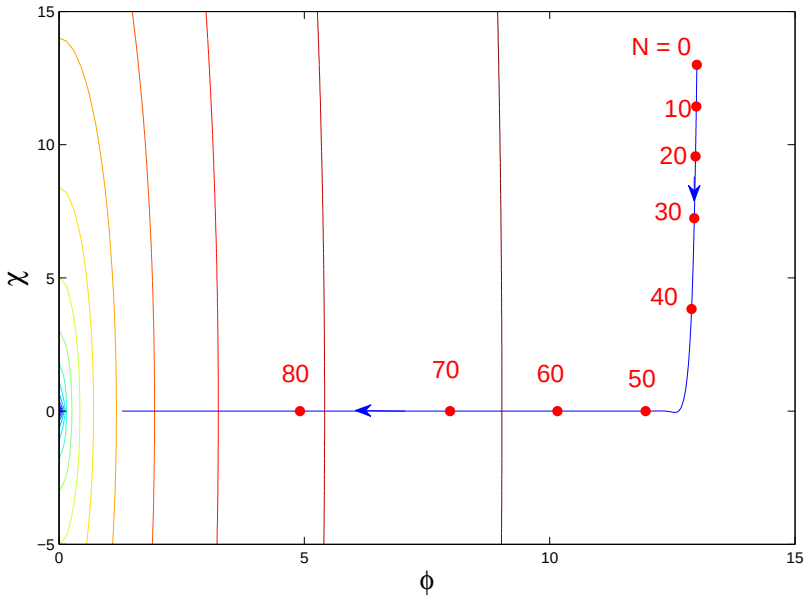

Figure 4–1: Detailed plot of the trajectory we examined in the case of quadratic two-field inflation (4.1), superimposed on a contour plot of the (logarithm of the) inflaton potential. Red dots represent time increments in e-folds.

before the end of inflation), in order to ascertain the scale-dependence of non-gaussianity. In the gauge $NH = 1$, modes are simply expressed:

$$k = k_0 e^{-t_*} \tag{4.2}$$

where k_0 is some reference mode. In the local case, we kept the squeezed (small k) mode constant, and varied the remaining two modes over the range of k.

4.1 Generic slow-roll trajectories

In contrast with the KKLT compactifiation, the large volume scenario places no strong restrictions on the value of W_0 in the effective field theory [15]. We were therefore free to vary the parameters that set the potential (2.21). Equations (3.75) and (3.73) were numerically integrated, first using

the parameter sets presented in [7]. Table 4–1 presents the parameter set used in this investigation. We simulated Roulette inflation trajectories starting from a variety of initial conditions and it was found that slow roll inflation was generically obtained, as mentioned in section 6 of [7], and as will be discussed in Section 4.2. In all cases the fields τ and θ were assumed to start at rest and were let to roll to the bottom of their potential. The simulation was terminated and inflation was assumed to finish as soon as the slow-roll condition broke down, *i.e.* as soon as $\log \epsilon = 0$. Some example trajectories are illustrated in Figure 4–2. Trajectory A, the "τ-valley" trajectory of Conlon and Quevedo [14], effectively corresponds to single-field inflation, as the fields start with θ already minimized. Figure 4–3 shows a more detailed plot of one of the trajectories, superimposed on a contour plot of the potential.

Values of ϵ were consistently very small, with $\log \epsilon \sim -13$ at the COBE scale. Typical values of the tensor-to-scalar ratio produced by the fields were therefore $r \simeq 3.5 \times 10^{-12}$.

Except when explicitly mentioned, all of the analyses of Roulette inflation were carried out with parameter set 1 of [7], but with the volume $\mathcal{V}$ tuned to achieve COBE normalisation ($\mathcal{V} = 8 \times 10^8 l_s^6$; see Table 4–1) such that the power spectrum (3.35) was $\sim 4 \times 10^{-10}$ on COBE scales, in order to compare the predictions of the model at this scale with observations. This resulted in inflation of order $V^{1/4} \simeq 10^{13}$ GeV, giving a nominal duration of approximately 65 e-foldings of inflation. Although a more generic method of normalization is to rescale the potential by an overall factor, the dependence on $1/\mathcal{V}$ of both terms in the potential gives a way to tune the potential without introducing additional parameters. In order to get a better idea of the effect of the various other parameters and initial conditions, we chose to normalize the potential

Table 4–1: Parameter set used for numerical simulations of the Roulette model. This corresponds to parameter set 1 of [7], but with $\mathcal{V}$ adjusted to meet COBE normalization - see section 4.3

W_0	a_2	A_2	λ_2	α	ξ	$\mathcal{V}$
300	$2\pi/3$	0.1	1	$1/9\sqrt{2}$	0.5	8×10^8

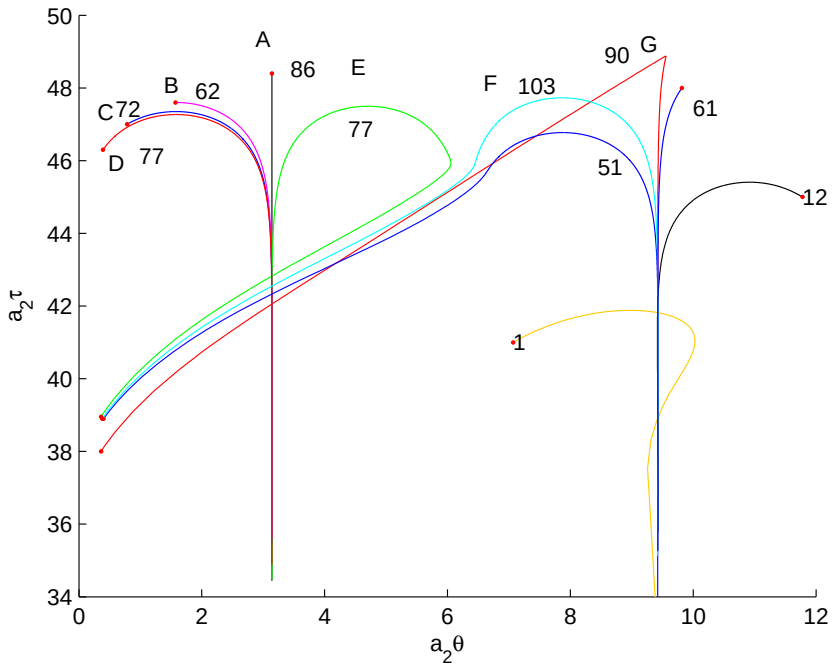

Figure 4–2: Various field trajectories for different intial field configurations (red dots). The numbers beside each curve are the number of efolds before the slow-rolling breaks down and ϵ exceedes 1. The potential here used the parameters from Table 4–1. The labeled trajectories A through G correspond to the ones referenced in table 4–2

only for one trajectory, corresponding to (effective one-field) slow-rolling in the τ-valley.

The number of e-foldings t_{end} before the end of inflation as well as the spectral tilt n_s were found to form smooth surfaces as functions of the initial values of τ and θ. Trajectories typically relaxed towards a τ valley minimum in the potential before rolling down the valley into one of the roulette pockets and ending inflation. At constant τ, initial configurations closer to the Conlon and Quevedo τ-valley ($\cos a_2\theta = -1$) rolled towards the minimum faster

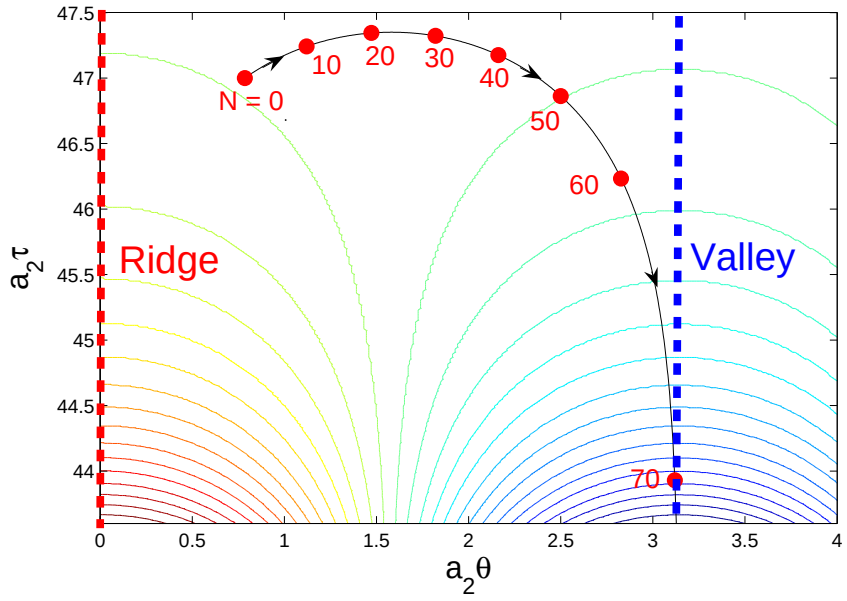

Figure 4–3: Detailed plot of trajectory C from Figure 4–2, superimposed on a contour plot of the inflaton potential. Red dots represent time increments in efolds.

and produced lower spectral indices when this quantity was computed with (3.36). Trajectories that started near the crest $\cos a_2\theta = 1$ did not allow for a graceful exit, given that the slope in the τ direction was large enough to push the volume modulus towards the exponentially flat region of stochastic self-reproduction, where quantum "kicks" dominate over classical rolling. For all parameter sets explored, the single-field estimate of n_s (figure 4–4) posessed minima $n_{s,min} = 0.96$ which were encountered for initial values of $a_2\theta$ corresponding to the respective extrema of the potential, in the θ direction. n_s was maximal at $a_2\theta = \pi/2, 3\pi/2, ...$ This behavior is quite unsurprising, given the explicit dependence of the spectral index on $\eta^{\|}$. With the exception of some highly exotic trajectories, the product $\dot{\theta}V_{,\theta}$ is always negative, making the tau valleys and crests respective maxima of $\eta^{\|}$. Within the τ-valley itself, it is shown in [14] that $\eta \approx -1/N_e$ where N_e is the number of e-foldings before the end of inflation and η is the standard single-field slow-roll parameter. The

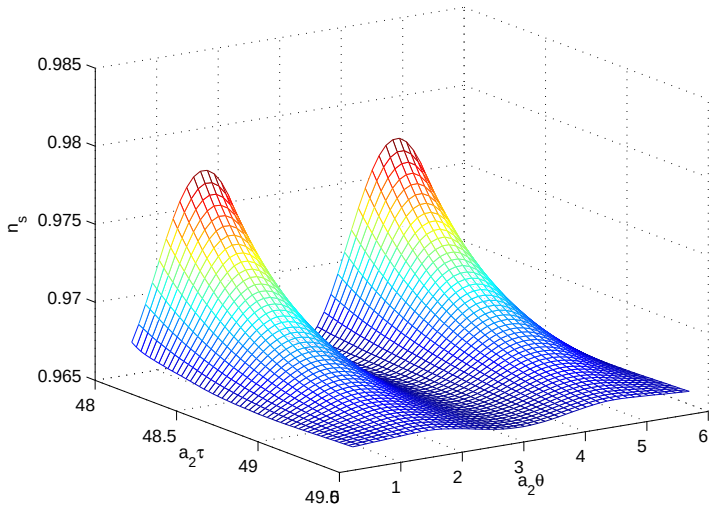

Figure 4–4: Spectral index n_s at COBE scale as a function of the initial field configuration, for a small range of initial conditions. This was calculated using the effective single-field result (3.37), without taking isocurvature modes into account. Note that the parameters used in this set of simulations do not correspond to the ones detailed in Table 4–1.

power spectrum for single-field, tau-valley inflation (trajectory A) was unaffected by isocurvature modes. Indeed, the power spectrum calculated using (3.36) was found numerically to agree with the power spectrum (3.104) evaluated at the end of inflation to within 0.3%. This indicates that entropy modes in the single-field case are very weakly coupled to the adiabatic direction, as expected, thus ensuring that the adiabatic fluctuations are frozen from horizon exit until reentry during radiation and matter domination, after the end of inflation.

In the case of more highly curved trajectories, however, the isocurvature modes were found to have a large, positive effect on the power spectrum of adiabatic perturbations, and consequently on the scalar spectral index n_s. This was observed in both models under consideration. Large curvature in field space during the course of inflation resulted in a "projection" of the

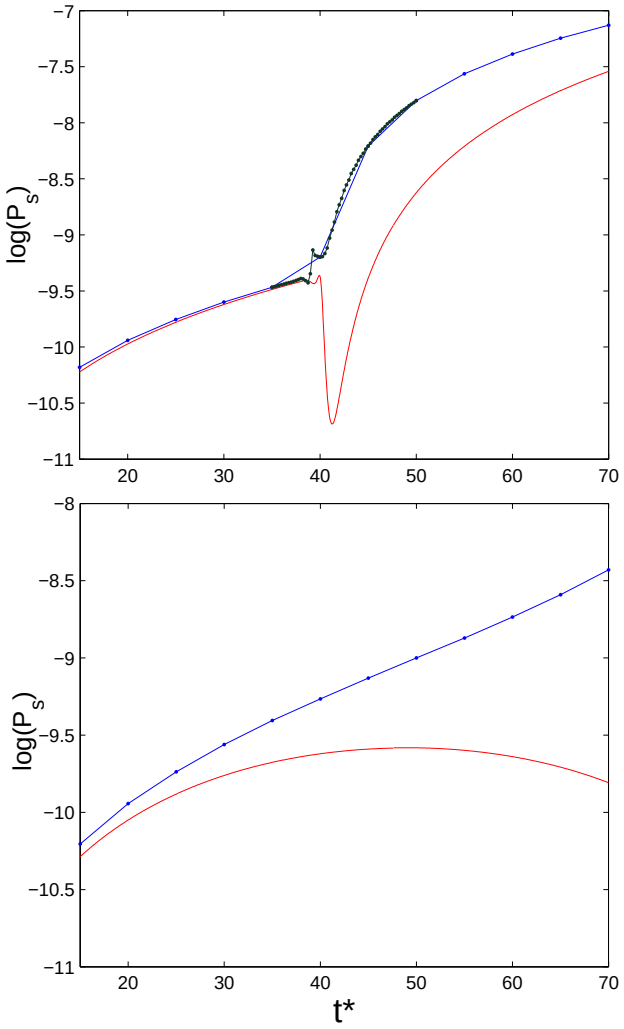

Figure 4–5: Effect of isocurvature modes during superhorizon evolution on the observed power spectrum at the end of inflation for two-field quadratic inflation (top, trajectory of figure 4–1) and Roulette inflation (bottom, trajectory C), as a function of k, where $t_*(k)$ is the time of horizon crossing of the corresponding mode k. In both cases the bottom (smooth red) line is the power spectrum computed with (3.36), while the top line is the full curvature power spectrum at the end of inflation after having considered the effect of entropy modes. Each point corresponds to a single numerical calculation.

isocurvature modes onto the adiabatic direction. The effect is most readily noticed in the context of the sharp turn in field space in the quadratic model investigated (Figure 4–5 left-hand pane), in which the modes generated after the curving show no deviation from the single-field prediction (3.36), while modes produced before the curve show a significantly higher power spectrum, along with a more red-tilted slope. In trajectories with long periods of curving, up to 75% of the power spectrum originated from the isocurvature modes. Table 4–2 gives the proportion of the observable curvature power spectrum at the end of inflation that results from the influence of isocurvature mode:

$$p^{\text{iso.}} \equiv \left| \frac{P_{\text{onefield}} - P_{\text{complete}}}{P_{\text{complete}}} \right|_{t_*=55}, \tag{4.3}$$

where the subscript $t_* = 55$ indicates that these quantities were evaluated roughly at COBE scale, for modes that crossed the horizon 55 efolds before the end of inflation. P_{onefield} is the power spectrum computed with (3.36), whereas P_{complete} was computed using (3.104). These results are in qualitative agreement with conclusions of ref. [24], although the latter study only examined a single trajectory in Roulette inflation. A second result of the influence of isocurvature modes (also mentioned by ref. [24]) is a lower scalar spectral index than would be naïvely expected from the single-field result (3.37). The full scalar spectral index n_s at COBE scales was computed by taking the derivative of a cubic fit of $\ln P_s$ (RMSE[1] < 0.05 in all cases), with the power spectrum evaluated from (3.104):

$$n_s^{(full)} = \frac{d \ln P_{\text{complete}}}{d \ln k} = \frac{d \ln P_{\text{complete}}}{dt}|_{t_*=55}. \tag{4.4}$$

[1] Root mean square error.

Table 4–2: Cosmological observables computed from chosen trajectories (Figure 4–2).

Trajectory	$\mathbf{a_2}\tau$	$\mathbf{a_2}\theta$	$\mathbf{f_{NL}^{equil.}}$	$\mathbf{f_{NL}^{squeezed}}$	$\mathbf{N}$	$\mathbf{n_s = -4\epsilon - 2\eta^{\parallel}}$	$\mathbf{n_s^{full}}$	$\mathbf{p}^{\mathrm{iso}}$
A	48.4	π	0	0	86	0.965	0.965	0
B	47.6	$\pi/2$	0.0052	0.0069	62	0.992	0.976	0.70
C	47.0	$\pi/4$	0.0105	0.0132	72	1.02	0.940	0.81
D	46.3	$\pi/8$	0.0242	0.0272	77	1.02	0.920	0.91
E	38.95	0.36	0.0688	0.0698	77	1.04	0.930	0.90
F	38.93	0.40	0.0068	0.0089	103	1.002	0.948	0.72
G	38	0.38	-0.0060	-0.0060	90	0.964	0.965	0.02

Here we have used the fact that in the gauge $NH = 1$ with $H \sim const.$,

$$\frac{d}{d\ln k} = \frac{d}{d\ln(aH)_*} \simeq \frac{d}{dt}. \tag{4.5}$$

Table 4–2 gives a comparison of both methods of computing n_s. Our results indicate that a significantly larger power spectrum, along with a generically red-tilted spectrum is an expected result of curved trajectories in Roulette inflation. This is of particular interest, given that most recent cosmological data favor a scalar spectral index of $n_s = 0.96$ [22].

4.2 Exploration of the parameter space

Starting with parameter set 1, we varied the different parameters of the potential (2.21) and the metric in field space $K_{2\bar{2}}$ one by one, in order to determine whether slow-roll inflation was indeed generically obtained in the model. Figure 4–6 illustrates our results. Trajectories starting below the solid red line would not give rise to sufficient inflation, whereas the inflaton evolution for trajectories that started above the dashed line would be dominated by quantum fluctuations rather than slow-rolling, giving rise to the never-ending "random walk" inflation of a self-reproducing universe. This region's limit was

found by numerically solving the condition (43) of [7]:

$$\frac{V}{12\pi^2} = \frac{1}{K_{2\bar{2}}}\left(\frac{V_{,\tau}}{V}\right)^2, \tag{4.6}$$

evaluated in the tau valley where $\cos(a_2\theta) = -1$.

For each parameter, the slope of minimum inflation (dashed blue) can be understood analytically: in the single field slow roll approximation, the number of e-folds from beginning t_i to end t_f of inflation is

$$N_e = \int_{t_i}^{t_f} H\ dt = \int_{t_i}^{t_f} \frac{H}{\partial\phi/\partial t} dt = \int_{\phi_f}^{\phi_i} \frac{V}{V'} d\phi \tag{4.7}$$

where ϕ is the canonically normalized inflaton, and we have used the slow-roll relations $3H\frac{\partial\phi}{\partial t} = -V'$ and $3H^2 = V$. In the single-field limit of roulette inflation, this gives [14]:

$$N_e = \frac{-3W_0\lambda_2\beta}{16\mathcal{V}^2 a_2^{3/2} A_2} \int_{a_2\tau_f}^{a_2\tau_i} \frac{e^{a_2\tau}}{\sqrt{a_2\tau}(1 - a_2\tau)} d(a_2\tau). \tag{4.8}$$

Here β is a parameter proportional to the uplift ΔV. For constant $N_e = 60$, the qualitative behavior of $a_2\tau_i$ as a function of each model parameter can be deduced from (4.8) without performing the integral. This behavior is in agreement with the numerical calculation of Figure 4–6.

The existence of slow-roll solutions was largely insensitive to variations of the Calabi-Yau volume $\mathcal{V}$; the complex structure contribution to the superpotential W_0; the scale of Kähler modulus λ_2; the gauge group associated with τ, a_2; along with the scale of the non-perturbative contribution of the Kähler potential, A_2. Note that a rescaling of α would have an identical effect to varying λ_2. Also note that the sign of W_0 is unimportant, as a change in its phase is exactly equivalent to a change in the phase of $a_2\theta$, which would simply correspond to a shift of the potential. Two important effects are worth pointing out: First, inflation cannot occur for volumes $\lesssim 2 \times 10^4$, using the

other parameters of set 1 and second, for integer N,

$$a_2 = 2\pi/N < 2\pi, \tag{4.9}$$

without which sufficient slow-roll inflation is impossible.

4.3 Nongaussianities in the Roulette model

Given recent claims of large isocurvature modes in the Roulette inflation model [24], and since nongaussianities in the curvature perturbations from superhorizon evolution are expected to be correlated with interaction with such entropy modes [37], one would naturally expect to find non-zero primordial bispectra from Roulette inflation. We therefore sought out deviations from gaussianity via the mechanism described in Section 3.3.

The algorithm for computing f_{NL} from superhorizon evolution of perturbation modes was benchmarked against two-field quadratic inflation, and was found to give identical results to [37]. This result is displayed in Figure 4–7. We then performed an analysis of non-linear mode evolution for a variety of Roulette inflation trajectories, and for a range of modes k corresponding to a range of horizon exit times $t_* = \ln k/H_*$ before the end of inflation. All of our nonlinearity analyses were carried out with parameter set 1, in the same way as the first-order analyses.

The Green's function in eq. (3.100) was found by solving the ODE numerically in matrix form, as a function of t. This was done once per time step t', giving a $3\times3\times M\times M$ dimensional array, where M corresponds to the number of discrete time steps sampled in the simulation of inflation (typically around 1000 were sufficient). The algorithm in Appendix A gives the exact details of this. Figure 4–8 illustrates the behavior of the components of $G_{ab}(t,t')$ for

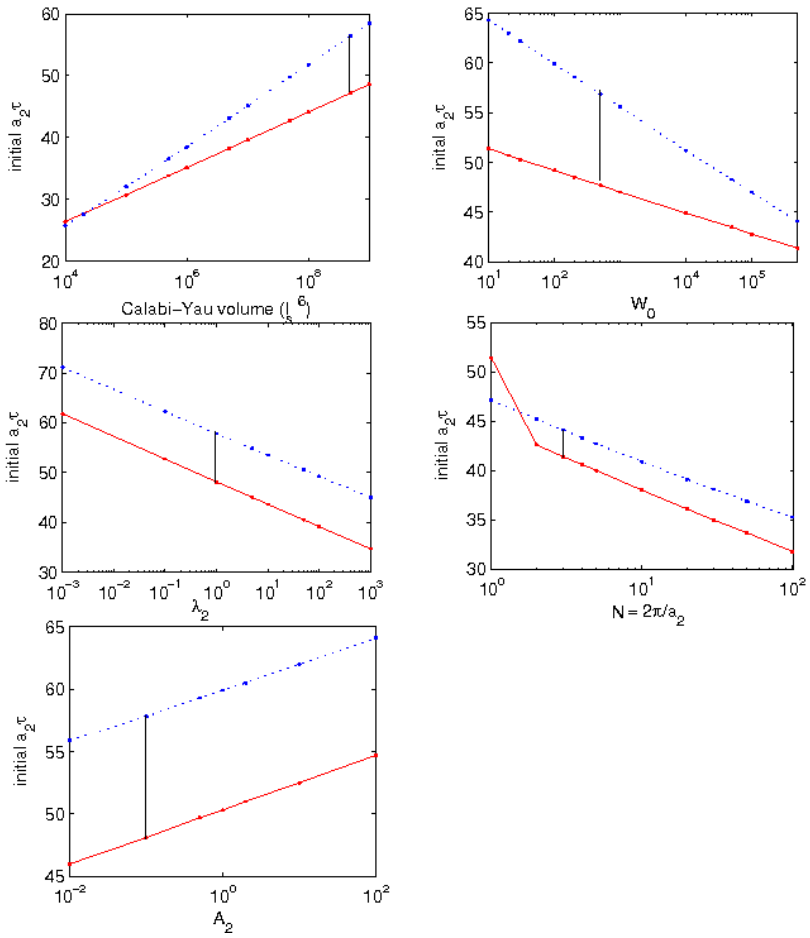

Figure 4–6: Effect of the variation of the different parameters of the potential (2.21) and field space metric (2.23) in Roulette inflation on the available space of initial conditions for inflation in the tau valley (single-field inflation). Solid lines represent the minimum initial value of $a_2\tau$ to obtain 60 e-folds of inflation, while the dashed lines are the beginning of the region of stochastic self-reproduction, where stochastic kicks dominate over the slope of the potential. Vertical lines indicate the values used in parameter set 1. Slow-roll inflation can only occur in the region bounded by the solid line from below, and the dashed line from above. In each case, the other parameters were kept constant.

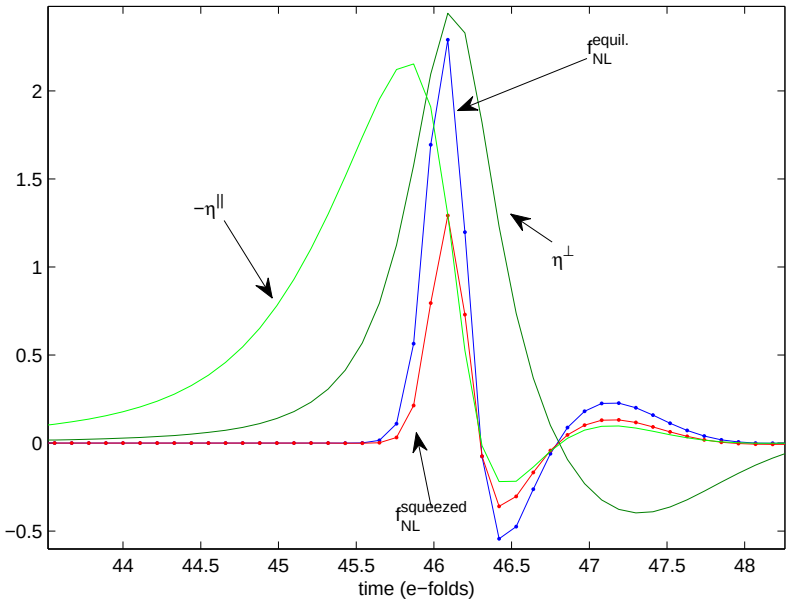

Figure 4–7: The non-linearity parameter f_{NL} as a function of time for the two-field quadratic model of eqn. (4.1), along with the parameters $\eta^{\perp}$ and $\eta^{\parallel}$, for the equilateral configuration ($t_*(k) = 60$ e-folds before the end of inflation) and the squeezed configuration, where the squeezed momentum left the horizon 20 e-folds earlier. This is in exact agreement with the results of ref. [37], albeit with a lower temporal resolution.

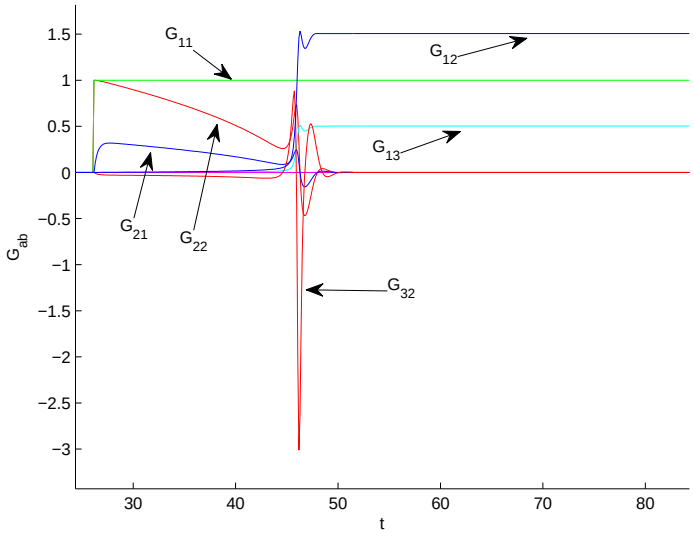

Figure 4–8: Green's functions $G_{ab}(t, t')$ for $t' = 60$ e-folds before the end of inflation, for $m_\phi^2\phi_1^2 + m_\chi^2\chi_2^2$ inflation with the parameters and trajectory given in the text. The nonzero components are labeled.

the two-field quadratic inflation, whereas Figure 4–9 shows this behavior for Roulette inflation.

Inflation in the τ valley, corresponding to the effective one-field scenario of Conlon and Quevedo [14] produced no nongaussianities originating from superhorizon interaction between scalar modes ($f_{NL} \sim 10^{-20}$, where the deviation from zero can be attributed to numerical uncertainty), as expected of this mechanism, since it is the coupling between curvature and isocurvature modes that is expected to generate large bispectra.[2] In more complex inflationary trajectories with sufficient curving in field space, however, values of f_{NL} between -0.01 and 0.02 were found to be quite generically produced,

[2] Recall that other contributions to f_{NL} should give values $\sim n_s - 1$ following (3.59).

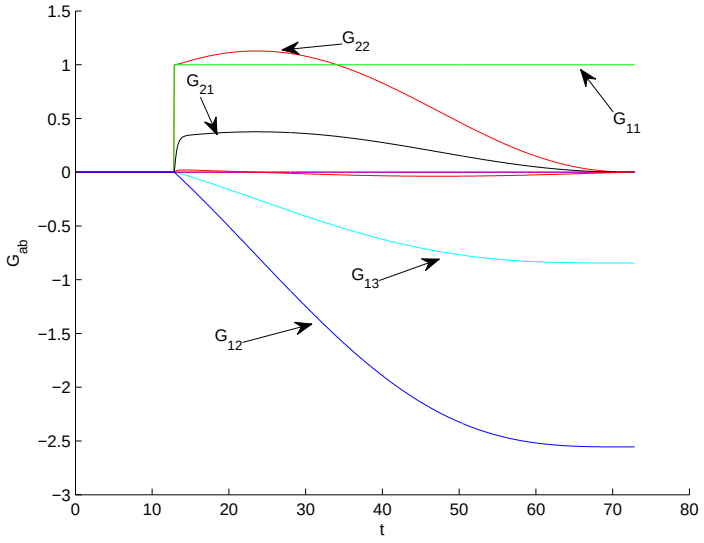

Figure 4–9: Green's functions $G_{ab}(t, t')$ for $t' = 60$ e-folds before the end of inflation, for Roulette inflation with the parameter set 1 and trajectory C. Only the nonzero components are labeled.

although the apparent limit:

$$|f_{NL}| \lesssim 0.1 \tag{4.10}$$

precludes detection of nongaussianities that would originate from this scenario.

For simple two-field quadratic inflation, strong curving in field space, usually associated with temporary breakdown of the slow-roll conditions [37] induces a temporary spike in the nonlinearity parameter f_{NL} for modes which exited the horizon before the curving event. This spike tends to vanish very quickly as slow rolling resumes, rendering the nonlinearity in the curvature modes unobservable after inflation. This is visible in figure 4–7.

Figure 4–10 illustrates the time-evolution of f_{NL} associated with certain wavemodes k from horizon exit to the end of inflation for a chosen trajectory of Roulette inflation (labeled C in figure 4–2), while figure 4–11 shows the k-dependence of f_{NL}. The behaviour of f_{NL} in general followed the type of evolution illustrated by trajectory C: most trajectories we examined that

curved during the period of observable inflation (i.e. in the last ~ 60 e-foldings) produced slightly more pronounced values of f_{NL} during curving, but these values quickly descended to $\sim 10^{-2}$ by the end of inflation. Table 4–2 gives some computed values of $f_{NL}^{equil.}$ of various other trajectories for $t_*(k) = 55$ e-foldings and of $f_{NL}^{squeezed}$ for k_1, k_2 and k_3 corresponding to $t_*(k_1) = 60$ and $t_*(k_2) = t_*(k_3) = 55$ respectively. Values of f_{NL} are taken at the end of inflation.

Features in $f_{NL}(k)$ can be identified with corresponding curvature of the trajectory at the time of horizon exit of particular modes. Modes that experienced more curving after horizon exit (*i.e.* modes that exited the horizon earlier) produced larger magnitude f_{NL} than those that experienced little or no effects of a change in background field direction of slow roll. These features in the bispectrum are completely absent in the context of single-field inflation. Should such precision ever be experimentally possible, the momentum dependence of f_{NL} would therefore provide a way of eliminating certain models of inflation, as well as certain trajectories in more complex multi-field models. One feature that was common to curved Roulette trajectories was a slightly larger bispectrum on large scales, corresponding to the modes which left the horizon before turning in field space occurred. A simultaneous detection of larger f_{NL} in the CMB and smaller primordial non-linearity in large-scale structure may be a way to detect this type of result, but this may only be possible in the context of models that predict larger f_{NL} from the onset.

The non-trivial field metric $K_{2\bar{2}}$ had no substantial effect on the shape, size, and magnitude of the bispectrum. Indeed, by taking the Roulette potential but with a canonically normalized kinetic term as a toy model, the spectrum of observables remained roughly unchanged.

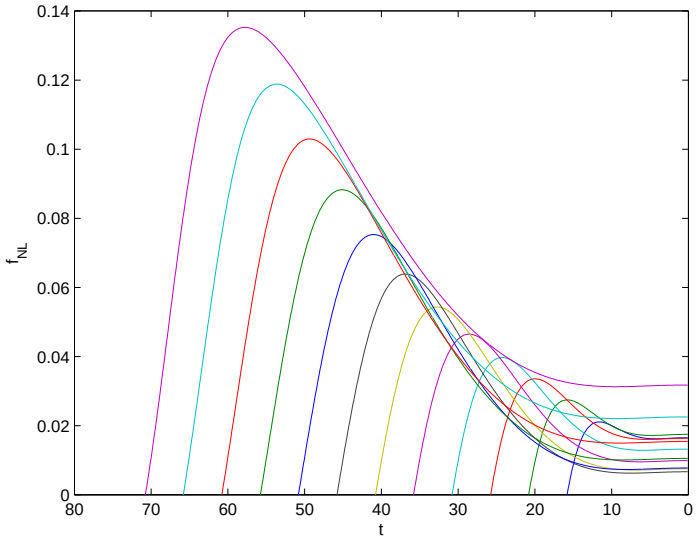

Figure 4–10: Time evolution of the non-linearity parameter f_{NL} for various modes, for trajectory C in the equilateral configuration. The beginning of each curve corresponds to $t = t_*$, the time of horizon crossing of the mode. Here, the x-axis is time until the end of inflation, in e-folds.

As illustrated in Table 4–2, the shape-dependence of the observed non-gaussianities was as expected from this type of model [1]. In all cases, the computed value of of f_{NL} was larger for the squeezed configuration than in the equilateral case.

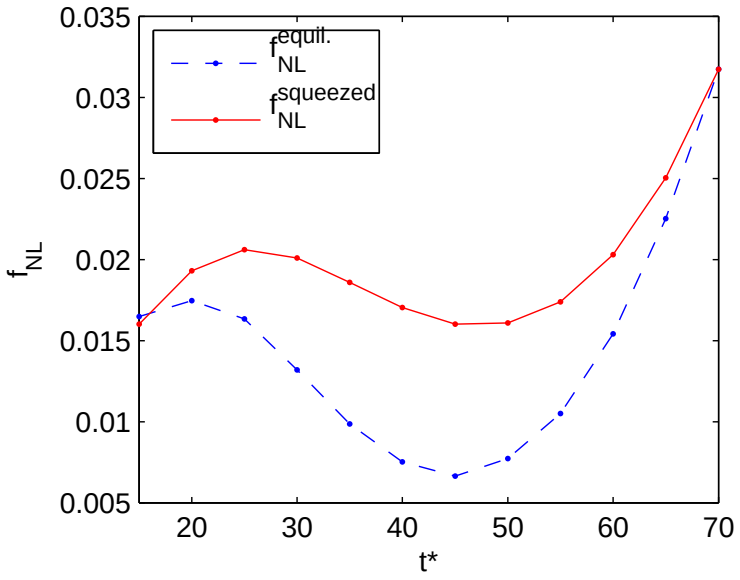

Figure 4–11: Momentum dependence of f_{NL} for trajectory C. The x-axis is the time of horizon crossing in e-folds of the corresponding mode, where $t_* = 0$ is the end of inflation. In the case of $f_{NL}^{squeezed}$ we took $t_{1*} = 70$ efolds. This is the reason that $f_{NL}^{equil.}(t_* = 70) = f_{NL}^{squeezed}(t_* = 70)$.

CHAPTER 5

Conclusions and future prospects

In the above, we have studied a model of Kähler moduli inflation built from a realistic construction of Type IIB string theory, and via the formalism developed in Chapter 3, we predicted a set of cosmological observables that would originate from various trajectories of inflation within this model; these include the power spectra and the superhorizon influence of isocurvature modes thereupon, as well as the deviations from Gaussianity of the predicted curvature spectrum that would originate from the superhorizon evolution of the curvature perturbation.

From the results obtained in Chapter 4, we may extract a few salient points. The first is that the Roulette scenario can, for a generous range of parameters tuned only to $O(1)$, drive a sufficient amount of inflation to solve the flatness and homogeneitiy problems for our universe.

When the full spectrum is considered, Roulette inflation furthermore predicts a smooth power spectrum with a slight red-tilt, in excellent agreement with estimates based on the latest WMAP data. In addition, as evidenced both from our study of Roulette inflation as well as a generic two-field quadratic

model, the superhorizon influence of isocurvature modes can come to dominate the scalar curvature power spectrum via the relation (3.55). This is the case for inflationary trajectories with large curvature, which can be imagined as a "projection" of the isocurvature perturbation modes onto the adiabatic direction. This contribution, which can account for up to 90% of the curvature power spectrum, must therefore be considered in the context of these multiple-field inflationary models.

A final conclusion concerns the deviations from Gaussianity of the curvature perturbation in the Roulette inflation model. It is unlikely that the levels of nongaussianity produced via the mechanism examined in Chapter 4 will be observable by future missions, given the small values of f_{NL} predicted, which are of the same order as nongaussianities expected from single-field inflation.

In light of our results, it would appear that the generation of a measurable, nonzero value of f_{NL} consistent with observations via this mechanism would require very sharp curving in field space, as in the trajectory studied in the context of two-field quadratic inflation in Chapter 4. Two further requirements make this difficult. First, if the trajectory immediately relaxes to a straight, effectively single-field trajectory, f_{NL} will damp to zero before the end of inflation, as illustrated in Figure 4–7. Slight curving up until the end of inflation in the Roulette trajectories we examined prevented this from happening completely within the latter scenario. Second, large deviation from Gaussianity from this method is correlated with large isocurvature modes being projected onto the curvature direction. In the presence of a model with large f_{NL}, one must therefore be careful that the power-spectrum is not overly amplified and distorted by this effect.

Should this mechanism produce sizeable f_{NL} within the context of a similar model, momentum-dependent bispectra would provide a good discriminator between models and inflationary trajectories within models. A way to measure this would be via the comparison of nongaussianities in the CMB with f_{NL} measured from Large Scale Structure surveys.

Further issues surrounding the Roulette model remain to be adressed. The initial conditions, which we took as free parameters to explore, require a mechanism to fix. For instance, this could be tunnelling from another configuration on a landscape of string theory solutions as discussed in ref. [7]. In this case, a proper Bayesian analysis of the prior probabilities would be required in order to get a full grip on the space of allowed initial conditions. In addition, it remains to be established whether the corrections (2.2) discussed in Chapter 2 are important, and whether they do indeed spoil the flatness of the potential.

It may be interesting to examine other such moduli inflation scenarios that arise once the assumptions of a strict hierarchy of scale are relaxed (for instance, the model of Ref.[2] in which the second dynamical field is the inverse overall volume, rather than the axionic partner). A more general study of two-field inflationary models with such an exponentially flat potential would furthermore reveal how generic the above-mentioned behavior is.

A full study of shape-dependence, as in Ref. [1] could also provide insight into the type of nongaussianities generated via this mechanism. As we hinted in Chapter 4, the squeezed configuration for f_{NL} generated slightly larger deviations from Gaussianity, but a full study of the dependence on k_1, k_2, k_3 could further constrain the microscopic parameters of this model. Although interesting from a purely theoretical point of view, the use of these results in comparison with data would of course be contingent upon both a successful

prediction of measurable f_{NL} and a successful shape-dependent measurement of f_{NL} in the CMB.

Although the development of ground-up models of inflation such as the Roulette scenario within string theory is an important step in reconciling the phenomenological paradigm of inflationary cosmology with fundamental microscopic physics, it equally important to develop proper discriminators to test these models against observations. The power spectrum and its tilt, as well as the bispectrum are among important observables in this respect; we have sought here to capsulize and apply some very powerful methods to compute these observables, including the relevant perturbation theory and the gradient expansion formalism of Rigopoulos, Shellard and van Tent in Chapter 3. We have shown that this formalism provides a relatively simple way to numerically compute the observables from any trajectory of models of multiple field inflation, and have thus predicted some key observables for the Roulette inflation model. With the advent of the Planck mission, as well as the nine-year data from the WMAP collaboration and the multitude of ground-based CMB experiments, it is clear that the next few years will represent a culmination of the so-called era of precision cosmology. It is with whetted anticipation that we await these results that will further bridge the gap between theory and observation.

Appendix A: numerical computation of observables

Following is the MATLAB code used to compute first and second-order quantities $v_{am}^{(1)}$ and $v_{amn}^{(2)}$, along with the k-dependent power spectrum and and the bispectrum in the equilateral triangle $k_1 = k_2 = k_3$ configuration. The required input, detailed in the commented section at the top of the script, was computed via numerical integration of the model under consideration (in this case two-field quadratic inflation and Roulette inflation). The important output variables are **PObsk** and **fNLk**, $m \times n$ arrays where m is the number of time-steps and n is the number of momenta for which observables were calculated. This algorithm was used to generate the results of Chapter 4, along with a similar computation in the squeezed k limit.

```
% nongauss2field2.m
%Final, working version. Fits perfectly with results from "Quantitative
%bispectra in two-field inflation"
%required input is recordN (vector of evenly-spaced time components),
%recordA (matrix A for each timestep), recordAbar (matrix \bar A for each
%time step), recordChi (vector of \chi), recordH (vector of Hubble parameter)
%calculates power spectrum and bispectrum from simulation results,
% for the equilateral case.

%initialize empty arrays.
c = 3;      %Window parameter. Result doesn't depend on this.
Xmx = [];
v1 = [];    %first order solution v
v1k = [];   %k-dependent version of v1.
powerSpectrumk = [];
PObsk = [];
%step three (just because steps one and two are nested)
%You only green once. Trust me. You only want to do this once.
sz = max(size(recordN));

if needG ==1
    opts = odeset(odeset,'RelTol',1e-8,'AbsTol',1e-11,'Vectorized','on');
```

```
%Use these for more precision
    global rA;
    global rN;
    rN = recordN';
    rA = permute(recordA,[3 1 2]); %watch out. Doing this so that the
%twoFieldGreen function works.

    masterG = zeros(3,3,sz,sz); %masterG(a b t t') are the correct indices
    for tprime = 1:sz-1

        %step one: get the green's function using builtin ODE solver.\
% Double-checked w/ ode45
        [T1,G1] = ode23(@twoFieldGreen,[recordN(tprime) recordN(sz)],[1 0 0]);
        [T2,G2] = ode23(@twoFieldGreen,[recordN(tprime) recordN(sz)],[0 1 0]);
        [T3,G3] = ode23(@twoFieldGreen,[recordN(tprime) recordN(sz)],[0 0 1]);

        %step two: reorganize it so it looks like it's supposed to

        G1 = interp1(T1,G1,recordN(tprime:sz));
        G2 = interp1(T2,G2,recordN(tprime:sz));
        G3 = interp1(T3,G3,recordN(tprime:sz));

        G = cat(3,G1',G2',G3'); %Good, but this isn't where I want my indices.
        G = permute(G,[1 3 2]);

        masterG(:,:,tprime:sz,tprime) = G;

        tprime %just a counter

    end
    needG = 0; %G won't be computed again until you rerun the simulation.
end


%%%%%%%%%Now we have the green's function %%%%%%%%%%
clear T1 T2 T3 G1 G2 G3 G;

for k = 2:max(size(recordChi))
    Xmx = cat(3,Xmx,[1 0; 0 1; 0 -recordChi(k)].*recordH(k)...
./sqrt(recordepsilon(k)));
end

% k-dependence is only important starting here.
%delay is the smoothing function bit in the delta function delta(t' - t_k +
%.5*log(2/c)
```

```
%delay is an integer

delay = round(.5*log(2/c^2)/freq/dN);

%     kOfInterest = 88;
fNLk = [];

for kOfInterest = 15:5:70
    v1 = [];
    v2 = [];
    tk = max(recordN) - kOfInterest;
    tkIndex = round(tk/(dN*freq));

    X = -1/2*Xmx;

    %As suggested by 0511041: take \dot{W} = \delta(kR/sqrt(2) - 1)
    %    %this is masterG_abtt*Xbmt, with contractions seemingly correct.
    % v(a,m,t)
    for t = 1:max(size(recordN))
                    v1 = cat(3,v1,masterG(:,:,t,tkIndex+delay)...
*X(:,:,tkIndex+delay));%no integration needed,
%since we've got a  delta
    end
    %first order adiabatic v:
    v11m = permute(v1(1,:,:),[2 3 1]);
    powerSpectrum = v11m(1,:).^2 + v11m(2,:).^2;
    powerSpectrumk = [powerSpectrumk; powerSpectrum];

    PObs = powerSpectrum*4/50/pi^2;  %this is the spectrum
% in terms of \delta_H

    %first order entropy v
    v12m = permute(v1(2,:,:),[2 3 1]);
    powerSpectrumEntropy = v12m(2,:).^2 + v12m(1,:).^2*25/18/pi^2;
    v13m = permute(v1(3,:,:),[2 3 1]);


%    v13m = permute(v1(3,:,:),[2 3 1]);
%
%

%%%%%%first order plots %%%%%%%%%%%%%%%%%%
% figure
% plot(recordN,powerSpectrum)
% hold on
```

```
% plot(recordN,powerSpectrumEntropy,'r')
% hold off

%%%%%%%%%%%%%%%%%%%%%%%%%%%%%%%%%%%%%%%%%%%%%%%%

%SECOND ORDER SOLUTION

%first bit of L
Lm1 = [recordEtaPerp.*v12m(1,:).*v11m(1,:);
 recordEtaPerp.*v12m(2,:).*v11m(1,:)]';
Lm2 = [recordEtaPerp.*v12m(1,:).*v11m(2,:);
 recordEtaPerp.*v12m(2,:).*v11m(2,:)]';

L = cat(3,Lm1,Lm2);
clear Lm1 Lm2

integrand = [];
grandintegrand = [];
masterGp = permute(masterG,[4 1 2 3]);
Abarp = permute(recordAbar,[4 1 2 3]);
v1p = permute(v1,[3 2 1]);
for t = 1:sz
    for m = 1:2
        for n = 1:2
            integrand1 = 0*(1:sz);
            for a = 1:3
                for b = 1:3
                    for d = 1:3
                        integrand1(:) = integrand1(:) + masterGp(:,1,a,t)...
                        .*Abarp(:,a,b,d).*v1p(:,m,b).*v1p(:,n,d);
                    end
                end
            end
            integrand(:,m,n) = integrand1(:);
        end
    end
    grandintegrand = cat(4,grandintegrand,integrand);
end

%    wind up with grandintegrand(tprime,m,n,t).
grandintegrand = permute(grandintegrand, [2 3 4 1]);
%    do the integraltrapz(recordN,grandintegrand,1)
integrated = 0*grandintegrand(:,:,:,1);
for t = 2:sz
    integrated(:,:,t) = trapz(recordN(1:t),grandintegrand(:,:,t,1:t),4);
```

```
end
integrated(:,:,1) = 0;
size(integrated)
integrated = permute(integrated,[3 1 2]);
LoL = L;
L = L - .5*integrated;

% Now I have L(m,n,t)-
f = 0*recordN;
for m = 1:2
    for n = 1:2
        f(:) = f(:) + L(:,m,n).*v11m(m,:)'.*v11m(n,:)';
    end
end
f = 2*f; %to account for k' <-> k

bispectrum = 3*f;  %equilateral triangle limit;
%without factor of (2pi)^3*delta(k+k'+k'')

fNL = bispectrum./(powerSpectrum.^2);
fNLk = cat(3,fNLk,fNL);
PObsk = [PObsk; PObs];
end
% figure
fNLk = permute(fNLk,[3 2 1]);
% plot(recordN,fNL)
```

```
function dG = twoFieldGreen(t,G)
%so t is actually an index, and not time. for the corresponding time take
%recordN(t)
% A = getVariable('A','global');
global rA;
global rN

dG = -getA(t)*G;

function fA = getA(t)
global rA;
global rN

 fA = permute(interp1(rN,rA,t),[2 3 1]); %proper approximation:
% lookup and interpolate. Default is linear.
```

References

[1] Daniel Babich, Paolo Creminelli, and Matias Zaldarriaga. The shape of non-Gaussianities. *JCAP*, 0408:009, 2004.

[2] Vijay Balasubramanian, Per Berglund, Raul Jimenez, Joan Simon, and Licia Verde. Topology from Cosmology. 2007.

[3] N. Barnaby, C. P. Burgess, and J. M. Cline. Warped reheating in brane-antibrane inflation. *JCAP*, 0504:007, 2005.

[4] Neil Barnaby and James M. Cline. Predictions for Nongaussianity from Nonlocal Inflation. 2008.

[5] Marcus Berg, Michael Haack, and Enrico Pajer. Jumping Through Loops: On Soft Terms from Large Volume Compactifications. *JHEP*, 09:031, 2007.

[6] J. J. Blanco-Pillado et al. Inflating in a better racetrack. *JHEP*, 09:002, 2006.

[7] J. Richard Bond, Lev Kofman, Sergey Prokushkin, and Pascal M. Vaudrevange. Roulette inflation with Kaehler moduli and their axions. *Phys. Rev.*, D75:123511, 2007.

[8] Evgeny I. Buchbinder, Justin Khoury, and Burt A. Ovrut. Non-Gaussianities in New Ekpyrotic Cosmology. *Phys. Rev. Lett.*, 100:171302, 2008.

[9] Philip Candelas and Xenia de la Ossa. Moduli Space of Calabi-Yau Manifolds. *Nucl. Phys.*, B355:455–481, 1991.

[10] Xingang Chen, Richard Easther, and Eugene A. Lim. Large non-Gaussianities in single field inflation. *JCAP*, 0706:023, 2007.

[11] M. Cicoli, C. P. Burgess, and F. Quevedo. Fibre Inflation: Observable Gravity Waves from IIB String Compactifications. 2008.

[12] James M. Cline. String cosmology. 2006.

[13] Joseph P. Conlon, Renata Kallosh, Andrei Linde, and Fernando Quevedo. Volume Modulus Inflation and the Gravitino Mass Problem. 2008.

[14] Joseph P. Conlon and Fernando Quevedo. Kaehler moduli inflation. *JHEP*, 01:146, 2006.

[15] Joseph P. Conlon, Fernando Quevedo, and Kerim Suruliz. Large-volume flux compactifications: Moduli spectrum and D3/D7 soft supersymmetry breaking. *JHEP*, 08:007, 2005.

[16] Paolo Creminelli, Leonardo Senatore, Matias Zaldarriaga, and Max Tegmark. Limits on f_{NL} parameters from WMAP 3yr data. *JCAP*, 0703:005, 2007.

[17] S. Dimopoulos, S. Kachru, J. McGreevy, and Jay G. Wacker. N-flation. 2005.

[18] Christopher Gordon, David Wands, Bruce A. Bassett, and Roy Maartens. Adiabatic and entropy perturbations from inflation. *Phys. Rev.*, D63:023506, 2001.

[19] Shamit Kachru, Renata Kallosh, Andrei Linde, and Sandip P. Trivedi. De Sitter vacua in string theory. *Phys. Rev.*, D68:046005, 2003.

[20] L. A. Kofman and D. Yu. Pogosian. Nonflat Perturbations in Inflationary Cosmology. *Phys. Lett.*, B214:508–514, 1988.

[21] E. Komatsu et al. First Year Wilkinson Microwave Anisotropy Probe (WMAP) Observations: Tests of Gaussianity. *Astrophys. J. Suppl.*, 148:119–134, 2003.

[22] E. Komatsu et al. Five-Year Wilkinson Microwave Anisotropy Probe (WMAP) Observations:Cosmological Interpretation. 2008.

[23] Eiichiro Komatsu and David N. Spergel. Acoustic signatures in the primary microwave background bispectrum. *Phys. Rev.*, D63:063002, 2001.

[24] Z. Lalak, D. Langlois, S. Pokorski, and K. Turzynski. Curvature and isocurvature perturbations in two-field inflation. *JCAP*, 0707:014, 2007.

[25] D. Langlois. Isocurvature cosmological perturbations and the CMB. *Comptes Rendus Physique*, 4:953–959, 2003.

[26] Hyun-Chul Lee, Misao Sasaki, Ewan D. Stewart, Takahiro Tanaka, and Shuichiro Yokoyama. A new delta N formalism for multi-component inflation. *JCAP*, 0510:004, 2005.

[27] Marilena LoVerde, Amber Miller, Sarah Shandera, and Licia Verde. Effects of Scale-Dependent Non-Gaussianity on Cosmological Structures. *JCAP*, 0804:014, 2008.

[28] David H. Lyth, Karim A. Malik, and Misao Sasaki. A general proof of the conservation of the curvature perturbation. *JCAP*, 0505:004, 2005.

[29] David H. Lyth and Antonio Riotto. Particle physics models of inflation and the cosmological density perturbation. *Phys. Rept.*, 314:1–146, 1999.

[30] Juan Martin Maldacena. Non-Gaussian features of primordial fluctuations in single field inflationary models. *JHEP*, 05:013, 2003.

[31] V. Mukhanov. Physical foundations of cosmology. Cambridge, UK: Univ. Pr. (2005) 421 p.

[32] V. Mukhanov and S. Winitzki. Introduction to quantum effects in gravity. Cambridge, UK: Univ. Pr. (2007) 273 p.

[33] J. A. Peacock. Cosmological physics. Cambridge, UK: Univ. Pr. (1999) 682 p.

[34] David Polarski and Alexei A. Starobinsky. Semiclassicality and decoherence of cosmological perturbations. *Class. Quant. Grav.*, 13:377–392, 1996.

[35] G. I. Rigopoulos, E. P. S. Shellard, and B. J. W. van Tent. Large non-Gaussianity in multiple-field inflation. *Phys. Rev.*, D73:083522, 2006.

[36] G. I. Rigopoulos, E. P. S. Shellard, and B. J. W. van Tent. Non-linear perturbations in multiple-field inflation. *Phys. Rev.*, D73:083521, 2006.

[37] G. I. Rigopoulos, E. P. S. Shellard, and B. J. W. van Tent. Quantitative bispectra from multifield inflation. *Phys. Rev.*, D76:083512, 2007.

[38] D. S. Salopek and J. R. Bond. Nonlinear evolution of long wavelength metric fluctuations in inflationary models. *Phys. Rev.*, D42:3936–3962, 1990.

[39] Misao Sasaki. Multi-brid inflation and non-Gaussianity. 2008.

[40] Misao Sasaki and Ewan D. Stewart. A General analytic formula for the spectral index of the density perturbations produced during inflation. *Prog. Theor. Phys.*, 95:71–78, 1996.

[41] David Seery and James E. Lidsey. Primordial non-gaussianities from multiple-field inflation. *JCAP*, 0509:011, 2005.

[42] Licia Verde, Li-Min Wang, Alan Heavens, and Marc Kamionkowski. Large-scale structure, the cosmic microwave background, and primordial non-gaussianity. *Mon. Not. Roy. Astron. Soc.*, 313:L141–L147, 2000.

[43] David Wands, Karim A. Malik, David H. Lyth, and Andrew R. Liddle. A new approach to the evolution of cosmological perturbations on large scales. *Phys. Rev.*, D62:043527, 2000.

[44] Amit P. S. Yadav and Benjamin D. Wandelt. Detection of primordial non-Gaussianity (fNL) in the WMAP 3-year data at above 99.5 2007.